41
6-2-82
Special Distr.
I-3481

WAPD-TM-1498
DOE RESEARCH AND
DEVELOPMENT REPORT

A FINITE-ELEMENT PROCEDURE FOR CALCULATING THE THREE-DIMENSIONAL INELASTIC BOWING OF FUEL RODS

(AWBA Development Program)

MASTER

S. E. MARTIN

DO NOT MICROFILM
COVER

MAY 1982

CONTRACT DE-AC11-76PN00014

DISTRIBUTION OF THIS DOCUMENT IS UNLIMITED

BETTIS ATOMIC POWER LABORATORY
PITTSBURGH, PENNSYLVANIA
Operated for the U. S. Department of Energy by
WESTINGHOUSE ELECTRIC CORPORATION

DISCLAIMER

This report was prepared as an account of work sponsored by an agency of the United States Government. Neither the United States Government nor any agency Thereof, nor any of their employees, makes any warranty, express or implied, or assumes any legal liability or responsibility for the accuracy, completeness, or usefulness of any information, apparatus, product, or process disclosed, or represents that its use would not infringe privately owned rights. Reference herein to any specific commercial product, process, or service by trade name, trademark, manufacturer, or otherwise does not necessarily constitute or imply its endorsement, recommendation, or favoring by the United States Government or any agency thereof. The views and opinions of authors expressed herein do not necessarily state or reflect those of the United States Government or any agency thereof.

DISCLAIMER

Portions of this document may be illegible in electronic image products. Images are produced from the best available original document.

DISCLAIMER

This book was prepared as an account of work sponsored by an agency of the United States Government. Neither the United States Government nor any agency thereof, nor any of their employees, makes any warranty, express or implied, or assumes any legal liability or responsibility for the accuracy, completeness, or usefulness of any information, apparatus, product, or process disclosed, or represents that its use would not infringe privately owned rights. Reference herein to any specific commercial product, process, or service by trade name, trademark, manufacturer, or otherwise, does not necessarily constitute or imply its endorsement, recommendation, or favoring by the United States Government or any agency thereof. The views and opinions of authors expressed herein do not necessarily state or reflect those of the United States Government or any agency thereof.

A FINITE-ELEMENT PROCEDURE FOR CALCULATING THE THREE-DIMENSIONAL INELASTIC BOWING OF FUEL RODS

(AWBA Development Program)

S. E. Martin

Contract No. DE-AC11-76-PN00014

WAPD-TM--1498

May 1982

DE82 015127

Printed in the United States of America
Available from the
National Technical Information Service
U. S. Department of Commerce
5285 Port Royal Road
Springfield, Virginia 22151

This document is an interim memorandum prepared primarily for internal reference and does not represent a final expression of the opinion of Westinghouse. When this memorandum is distributed externally, it is with the express understanding that Westinghouse makes no representation as to completeness, accuracy, or usability of information contained herein.

BETTIS ATOMIC POWER LABORATORY PITTSBURGH, PENNSYLVANIA 15122-0079

Operated for the U.S. Department of Energy
by WESTINGHOUSE ELECTRIC CORPORATION

DISTRIBUTION OF THIS DOCUMENT IS UNLIMITED

NOTICE

This report was prepared as an account of work sponsored by the United States Government. Neither the United States, nor the United States Department of Energy, nor any of their employees, nor any of their contractors, subcontractors, or their employees, makes any warranty, express or implied, or assumes any legal liability or responsibility for the accuracy, completeness or usefulness of any information, apparatus, product or process disclosed, or represents that its use would not infringe privately owned rights.

FOREWORD

The Shippingport Atomic Power Station located in Shippingport, Pennsylvania was the first large-scale, central-station nuclear power plant in the United States and the first plant of such size in the world operated solely to produce electric power. This program was started in 1953 to confirm the practical application of nuclear power for large-scale electric power generation. It has provided much of the technology being used for design and operation of the commercial, central-station nuclear power plants now in use.

Subsequent to development and successful operation of the Pressurized Water Reactor in the Atomic Energy Commission (now Department of Energy, DOE) owned reactor plant at the Shippingport Atomic Power Station, the Atomic Energy Commission in 1965 undertook a research and development program to design and build a Light Water Breeder Reactor core for operation in the Shippingport Station.

The objective of the Light Water Breeder Reactor (LWBR) program has been to develop a technology that would significantly improve the utilization of the nation's nuclear fuel resources employing the well-established water reactor technology. To achieve this objective, work has been directed toward analysis, design, component tests, and fabrication of a water-cooled, thorium oxide-uranium oxide fuel cycle breeder reactor for installation and operation at the Shippingport Station. The LWBR core started operation in the Shippingport Station in the Fall of 1977 and will finish routine power operation on October 1, 1982. After End-of-Life core testing, the core will be removed and the spent fuel shipped to the Naval Reactors Expended Core Facility for detailed examination to verify core performance including an evaluation of breeding characteristics.

In 1976, with fabrication of the Shippingport LWBR core nearing completion, the Energy Research and Development Administration, now DOE, established the Advanced Water Breeder Applications (AWBA) program to develop and disseminate technical information which would assist U. S. industry in evaluating the LWBR concept for commercial-scale applications. The AWBA program, which is concluding in September, 1982, has explored some of the problems that would be faced by industry in adopting technology confirmed in the LWBR program. Information already developed includes concepts for commercial-scale prebreeder cores which would produce uranium-233 for light water breeder cores while producing electric power, improvements for breeder cores based on the technology developed to fabricate and operate the Shippingport LWBR core, and other information and technology to aid in evaluating commercial-scale application of the LWBR concept.

All three development programs (Pressurized Water Reactor, Light Water Breeder Reactor, and Advanced Water Breeder Applications) have been conducted under the technical direction of the Office of the Deputy Assistant Secretary for Naval Reactors of DOE.

Technical information developed under the Shippingport, LWBR, and AWBA programs has been and will continue to be published in technical memoranda, one of which is this present report.

TABLE OF CONTENTS

ABSTRACT

A Finite Element Procedure for Calculating the Three-Dimensional Inelastic Bowing of Fuel Rods

An incremental finite element procedure is developed for calculating the in-pile lateral bowing of nuclear fuel rods. The fuel rod is modeled as a viscoelastic beam whose material properties are derived as perturbations of the results of an axisymmetric stress analysis of the fuel rod. The effects which are taken into account in calculating the rod's lateral bowing include: (a) lateral, axial, and rotational motions and forces at the rod supports, (b) transverse gradients of temperature, fast-neutron flux, and fissioning rate, and (c) cladding circumferential wall thickness variation. The procedure developed in this report could be used to form the basis for a computer program to calculate the time-dependent bowing as a function of the fuel rod's operational and environmental history.

A Finite Element Procedure for Calculating the Three-Dimensional Inelastic Bowing of Fuel Rods

(AWBA Development Program)

S. E. Martin

I. Introduction

In most commercial nuclear power reactors, cylindrical or annular fuel pellets are stacked within long closed-ended metal tubes, called the cladding, which isolate the fuel from the coolant. Such a fuel-cladding assemblage constitutes a fuel rod. Within the reactor core, a fuel rod is held in position at intervals along its length by supports, usually referred to as grids. During normal reactor operation, various factors can cause the fuel rod to bend, or bow, laterally. This bowing can be induced by transverse temperature gradients in the fuel rod, transverse fast-neutron flux gradients, axial loads on the fuel rod, cladding wall thickness circumferential variations, and grid support motion.

A method for calculating the time-dependent two-dimensional inelastic bowing of fuel rods was developed in [1]* and implemented in the ROBOT computer program [2]. The analysis was two-dimensional in the sense that it was assumed that the rod configuration and displacements were restricted to a single plane. In the method developed in [1], the rod lateral deflection in each span is approximated by a polynomial and the deflection is solved for using the Galerkin method [3]. To perform a rod bowing analysis, the analyst first runs the CYGRO computer program [4] to calculate the axisymmetric stresses, temperatures, and material states within the fuel rod as a function of time. This information is then used by the ROBOT computer program to calculate the time-dependent fuel rod bowing.

The axial forces in an axially restrained fuel rod are related to the lateral deflections of the rod because bowing tends to shorten the chord length of the rod. Although the assumption that the bowing is two-dimensional may sometimes be a good approximation, in general the bowing

---

* Throughout this report, numbers in brackets denote items in the list of References. Numbers in parenthesis denote the equations included in the text.

is three-dimensional in nature; that is, the rod is deformed into a space curve which cannot be contained in a single plane. In this case the axial shortening of the rod with bowing depends on both components of the lateral deflection and a single-plane analysis of this type of problem does not accurately model the axial-lateral interaction.

In this report the analysis developed in [1] is extended so that three-dimensional bowing can be analyzed. Both components of the rod's lateral deflection are calculated simultaneously and therefore the interaction between the axial displacements and the lateral displacements is more accurately modeled. The analysis developed here forms the basis for a computer program to calculate fuel rod bowing. In order to simplify the analysis and significantly reduce the computer run time, the variational method used in [1] is replaced here with a finite element formulation. The computer run time should be reduced because the structure stiffness matrix which is obtained is symmetric, positive-definite, and narrowly banded. This means that the structural stiffness equations can be rapidly solved using a Cholesky equation-solver [5]. In addition to the above modifications, the analysis is extended so that the bowing of fuel rods containing duplex fuel can be analyzed. With duplex fuel, the fuel pellet is generally made of two materials —— an annular or cylindrical pellet consisting of one material surrounded by an annular pellet made of another material. This type of fuel is currently under development for use in water breeder reactors.

The rod incremental finite element equations are formulated in Section II. When solved, these equations determine the time-dependent lateral and axial deformation of the fuel rod in terms of the support motions and the transverse fast-neutron flux and temperature gradients. These gradients, and the support locations and motions, would be user-supplied input to a computer program based on this method.

To formulate the incremental finite element equations, it is necessary to know the incremental moment-curvature and axial force-strain relations of the fuel rod. These relations can be derived from a knowledge of the fuel rod material properties, the axisymmetric temperature distribution, and the axisymmetric state of stress and deformation in the fuel rod. This information is obtained from a data file written by the CYGRO computer program and is generated prior to performing the rod bowing analysis. The calculation of the fuel rod moment-curvature and axial force-strain relations from this data is described in

Section III. The moment-curvature relations also contain terms which represent moment-free curvatures which can be induced in the fuel rod by a number of different mechanisms. In Section IV, all such mechanisms which are currently known are discussed and expressions for the corresponding induced curvatures are given.

In general, the initial free shape of a fuel rod is not straight and it is necessary to fit the initial shape of the rod to a set measured deflection data. A procedure for obtaining a modified least-squares fit to the data using the finite element shape functions is given in Section V. The advantage of the new method is that there are very few restrictions placed on either the number or the locations of the data points.

Notation

In what follows, both matrix and matrix shorthand, or direct, notation will be used. For example, $\underline{a}$ will denote that the quantity a is a vector, or one-dimensional matrix, and $\underset{\sim}{a}$ will denote that a is a matrix of more than one dimension. $\underset{\sim}{a}^T$ will denote the transpose of the matrix $\underset{\sim}{a}$ and $\underset{\sim}{a}^{-1}$ will denote its inverse. A bending moment is designated M^x if it tends to cause bending in the x-z plane and designated M^y if it tends to cause bending in the y-z plane.

II. The Finite Element Equations

In this section the method of virtual work is used to derive the incremental finite element equations. This method is equivalent to the Galerkin method used in [1] and is somewhat more intuitive. To apply the method of virutal work, expressions for the rod's external and internal work rates must first be derived from the rod's equilibrium differential equations. After this is done in Section A, the incremental finite element stiffness equations are formulated in Section B and the element assembly procedure is described in Section C. Section D discusses the imposition of boundary conditions and Section E outlines the procedure for back-calculating the stresses and strains in the element.

A. The Energy Equation

In this analysis, the fuel rod is modeled as a viscoelastic beam which is supported at discrete points along its length. Figure 1 shows the forces and moments which act on a differential element of the beam. The z direction is taken to be along the beam and the x and y directions are transverse to the beam. Figure 1 also indicates the directions which are taken as positive for the various forces and moments. By summing the appropriate forces and moments to zero, we obtain

$$(S^x)' + q^x = 0 \quad , \tag{2.1}$$

$$(S^y)' + q^y = 0 \quad , \tag{2.2}$$

$$(M^x)' + S^x - Tu' = 0 \quad , \tag{2.3}$$

$$(M^y)' + S^y - Tv' = 0 \quad , \tag{2.4}$$

$$T' + q^z = 0 \quad , \tag{2.5}$$

where M^x and M^y are the moments acting within the beam, q^x, q^y and q^z are the distributed forces acting on the beam, u and v are the x- and y-displacements respectively, T is the axial force, S^x and S^y are the x- and y-direction shear forces respectively, and a prime denotes differentiation with respect to z. From Equations (2.1)-(2.5), the differential equations of equilibrium can be written in the form

$$Tu'' + q^x - (M^x)'' - q^z u' = 0 \tag{2.6}$$

$$Tv'' + q^y - (M^y)'' - q^z v' = 0 \tag{2.7}$$

$$T' + q^z = 0 \tag{2.8}$$

To obtain the energy rate equation, multiply (2.6) by $\dot{u}$, (2.7) by $\dot{v}$, (2.8) by $\dot{w}$, and add to obtain

$$Tu'' \dot{u} + q^x \dot{u} - (M^x)'' \dot{u} - q^z u' \dot{u} + Tv'' \dot{v} + q^y \dot{v} - (M^y)'' \dot{v} - q^z v' \dot{v} + T' \dot{w} + q^z \dot{w} = 0 \tag{2.9}$$

where w is the z-direction displacement and where a superposed dot denotes differentiation with respect to time. After some manipulation, Equation (2.9) can be written in the form

$$\frac{d}{dz}\left[S^{x}\dot{u} + M^{x}\dot{u}' + S^{y}\dot{v} + M^{y}\dot{v}' + T\dot{w}\right] + \left[q^{x}\dot{u} + q^{y}\dot{v} + q^{z}\dot{w}\right]$$

$$= \left[M^{x}\dot{u}'' + M^{y}\dot{v}'' + T\dot{\epsilon}\right] \tag{2.10}$$

where ϵ is the axial strain in the rod and is given by

$$\epsilon = w' + \frac{1}{2}(u')^2 + \frac{1}{2}(v')^2. \tag{2.11}$$

Equation (2.11) shows that the axial strain in the rod depends upon both the axial and the lateral displacements. If the z-displacements are zero, the lateral displacements can still induce an axial strain in the rod. Thus, Equation (2.11) represents a nonlinear coupling between the axial and lateral displacements.

We now consider a finite segment of length ℓ and integrate Equation (2.10) over this segment to obtain

$$\left[S^{x}\dot{u} + M^{x}\dot{u}' + S^{y}\dot{v} + M^{y}\dot{v}' + T\dot{w}\right]\Big|_{o}^{\ell}$$

$$+ \int_{o}^{\ell}\left[q^{x}\dot{u} + q^{y}\dot{v} + q^{z}\dot{w}\right] dz$$

$$= \int_{o}^{\ell}\left[M^{x}\dot{u}'' + M^{y}\dot{v}'' + T\dot{\epsilon}\right] dz \quad . \tag{2.12}$$

The left-hand side of Equation (2.12) represents the work rate of the external forces acting on the rod segment. The first term in brackets represents the work rate by forces and moments applied at the ends of the rod segment and the second term represents the work rate of the distributed external forces. The right-hand side of Equation (2.12) is the internal work rate. If we define the stress and strain* to be the vectors $\underline{\sigma}$ and $\underline{\varepsilon}$ given by

---

* Note that the quantities referred to here as "stress" and "strain" are not stresses and strains in the usual terminology of solid mechanics. These terms are used because the quantities defined here play the same role in the finite element scheme developed here as the usual definitions of stress and strain play in a finite element model of a solid continuum.

$$\underline{\sigma} = \begin{bmatrix} M^x \\ M^y \\ T \end{bmatrix}, \quad \text{and} \quad \underline{\varepsilon} = \begin{bmatrix} u'' \\ v'' \\ \epsilon \end{bmatrix}, \tag{2.13}$$

the internal work rate can be written

$$\dot{W}_{int} = \int_o^\ell \dot{\underline{\varepsilon}}^T \underline{\sigma} \, dz \quad . \tag{2.14}$$

The external work rate can also be expressed more compactly in matrix form as

$$\dot{W}_{ext} = \dot{\underline{P}}^T \underline{F} + \int_o^\ell \dot{\underline{U}}^T \underline{b} \, dz \tag{2.15}$$

where

$$\underline{U} = \begin{bmatrix} u \\ v \\ w \end{bmatrix}, \quad \underline{b} = \begin{bmatrix} q^x \\ q^y \\ q^z \end{bmatrix} \tag{2.16}$$

and where $\underline{P}$ and $\underline{F}$ are vectors of generalized displacement and force having components defined by

$$\begin{aligned}
P_1 &= u \text{ at left end,} \\
P_2 &= u' \quad " \quad , \\
P_3 &= v \quad " \quad , \\
P_4 &= v' \quad " \quad , \\
P_5 &= w \quad " \quad , \\
P_6 &= u \text{ at right end,} \\
P_7 &= u' \quad " \quad , \\
P_8 &= v \quad " \quad , \\
P_9 &= v' \quad " \quad , \\
P_{10} &= w \quad " \quad ,
\end{aligned} \tag{2.17}$$

and

$$
\begin{aligned}
F_1 &= F^x \quad \text{at left end} , \\
F_2 &= M^x \quad " \quad , \\
F_3 &= F^y \quad " \quad , \\
F_4 &= M^y \quad " \quad , \\
F_5 &= F^z \quad " \quad , \\
F_6 &= F^x \quad \text{at right end} , \\
F_7 &= M^x \quad " \quad , \\
F_8 &= F^y \quad " \quad , \\
F_9 &= M^y \quad " \quad , \\
F_{10} &= F^z \quad " \quad .
\end{aligned}
\tag{2.18}
$$

The positive directions for the applied external forces and moments are shown in Figure 2*.

Using the expressions (2.14) and (2.15) for the internal and external work rates, the energy rate equation, Equation (2.12), can be written

$$\underline{\dot{P}}^T \underline{F} + \int_o^\ell \underline{\dot{U}}^T \underline{b} \, dz = \int_o^\ell \underline{\dot{\varepsilon}}^T \underline{\sigma} \, dz \ . \tag{2.19}$$

This equation expresses the balance between the internal and external energy rates for quasi-static processes.

B. The Element Stiffness Equation

In this section the expressions for the internal and external work rates derived above are used in conjunction with the assumed displacement shape functions to derive the element stiffness equation. It is assumed that the rod is divided into a set of contiguous segments which are the finite elements. The two endpoints of each finite element are its nodes. The set of shapes which the rod segment can actually assume

* To obtain (2.15) from (2.12) it is necessary to keep in mind that internal forces and moments acting on the left end of the rod segment have a positive sense which is opposite to the positive sense assumed for the external forces and moments.

can be regarded as an infinite-dimensional function space (a Hilbert space). In the finite element method, this infinite-dimensional space is approximated by a finite-dimensional space. That is, it is assumed that the shape of the finite element can be written as a linear combination of a finite set of basis functions called shape functions. In particular, it is assumed here that the shape of the finite element can be approximated by

$$\begin{bmatrix} u \\ v \\ w \end{bmatrix} = \begin{bmatrix} S_1 & S_2 & 0 & 0 & 0 & S_3 & S_4 & 0 & 0 & 0 \\ 0 & 0 & S_1 & S_2 & 0 & 0 & 0 & S_3 & S_4 & 0 \\ G_1 & G_2 & G_3 & G_4 & G_5 & G_6 & G_7 & G_8 & G_9 & G_{10} \end{bmatrix} \begin{bmatrix} P_1 \\ P_2 \\ P_3 \\ P_4 \\ P_5 \\ P_6 \\ P_7 \\ P_8 \\ P_9 \\ P_{10} \end{bmatrix} \tag{2.20}$$

or

$$\underline{U} = \underset{\sim}{S}\,\underline{P}$$

where $\underline{U}$ and $\underline{P}$ are defined by (2.16) and (2.17), and where

$$S_1 = 1-3(z/\ell)^2 + 2(z/\ell)^3$$

$$S_2 = \ell[(z/\ell) - 2(z/\ell)^2 + (z/\ell)^3]$$

$$S_3 = 3(z/\ell)^2 - 2(z/\ell)^3$$

$$S_4 = \ell[- (z/\ell)^2 + (z/\ell)^3]$$

where ℓ is the element length and z is a local coordinate which assumes a value of zero at the left node and a value of ℓ at the right node. The functions S_1 through S_4 and G_1 through G_{10} are called the shape functions and the matrix $\underset{\sim}{S}$ is called the shape matrix. The functions S_1 through S_4 are the Hermitian polynomials and are commonly used in beam-type problems [6].

In most problems of practical interest, the axial strain in the fuel rod will be nearly uniform over lengths which are modeled by a single finite element. Therefore, the axial shape functions G_1 through G_{10} will be defined so as to make the axial strain uniform within the element. To derive the forms of these functions, we assume that the axial strain ϵ given by Equation (2.11) is uniform (i.e. does not vary with z) and solve for w' to obtain

$$w'(z) = \epsilon - \frac{1}{2}\left[(u')^2 + (v')^2\right]$$

To solve for the axial displacement w(z), we integrate this equation with respect to z to obtain

$$w(z) = \epsilon\, z - \frac{1}{2}\int \left[(u')^2 + (v')^2\right] dz + k \qquad (2.21)$$

where k is the integration constant. Using the shape functions for the lateral displacements, u' and v' can be written

$$u' = \sum_{i=1}^{10} S'_{1i}\, P_i \quad , \quad v' = \sum_{i=1}^{10} S'_{2i}\, P_i \qquad (2.22)$$

where S_{ji} represents the shape function in the jth row and ith column of the shape matrix. Substituting these expressions for u' and v' into Equation (2.21) gives

$$w(z) = \epsilon\, z - \sum_{i=1}^{10}\sum_{j=1}^{10} A_{ij}\, P_i\, P_j + k \qquad (2.23)$$

where the matrix A_{ij} is given by

$$A_{ij} = \frac{1}{2} \int [S'_{1i} S'_{1j} + S'_{2i} S'_{2j}] \, dz \, . \tag{2.24}$$

The w displacements at the ends of the element are the axial nodal displacements P_5 and P_{10}, that is

$$w(0) = P_5 \quad \text{and} \quad w(\ell) = P_{10} \, .$$

Substituting $z = 0$ and $z = \ell$ into Equation (2.23), we get the two equations

$$P_5 = k$$

$$P_{10} = \epsilon \ell - \sum_{i=1}^{10} \sum_{j=1}^{10} A_{ij}(\ell) P_i P_j + k$$

where the fact that $A_{ij}(0) = 0$ has been used. From these two equations we can solve for the strain ϵ and the integration constant k to obtain

$$k = P_5 \tag{2.25}$$

$$\epsilon = (1/\ell) \left[P_{10} - P_5 + \sum_{i=1}^{10} \sum_{j=1}^{10} A_{ij}(\ell) P_i P_j\right] . \tag{2.26}$$

Substituting these back into (2.23), we get

$$w(z) = (1/\ell) \left[P_{10} - P_5 + \sum_{i=1}^{10} \sum_{j=1}^{10} A_{ij}(\ell) P_i P_j\right] z$$

$$- \sum_{i=1}^{10} \sum_{j=1}^{10} A_{ij}(z) P_i P_j + P_5 \, . \tag{2.27}$$

This equation can be written in the form

$$w(z) = \sum_{i=1}^{10} G_i P_i \tag{2.28}$$

where the G_i functions are the axial shape functions and are given by

$$G_i(z) = (z/\ell) \sum_{j=1}^{10} A_{ij}(\ell) P_j - \sum_{j=1}^{10} A_{ij}(z) P_j \quad \text{if} \quad i \neq 5 \text{ or } 10$$

$$G_5(z) = [1 - (z/\ell)] , \quad G_{10}(z) = (z/\ell) .$$

Use of these axial shape functions ensures that the axial strain within the element will be uniform regardless of the lateral deflections.

Using Equation (2.20) and Equation (2.26), the strain vector defined by (2.13) is given by

$$\underline{\varepsilon} = \hat{\underset{\sim}{B}}\, \underline{P} \tag{2.29}$$

where $\hat{\underset{\sim}{B}}$ is the strain matrix, given by

$$\hat{\underset{\sim}{B}} = \begin{bmatrix} S_1'' & S_2'' & 0 & 0 & 0 & S_3'' & S_4'' & 0 & 0 & 0 \\ 0 & 0 & S_1'' & S_2'' & 0 & 0 & 0 & S_3'' & S_4'' & 0 \\ J_1 & J_2 & J_3 & J_4 & J_5 & J_6 & J_7 & J_8 & J_9 & J_{10} \end{bmatrix} \tag{2.30}$$

where

$$J_j = (1/\ell) \sum_{i=1}^{10} A_{ij}(\ell) P_i \quad \text{if} \quad j \neq 5 \text{ or } 10 \tag{2.31}$$

$$J_5 = - (1/\ell) \quad , \quad J_{10} = (1/\ell) . \tag{2.32}$$

The strain rate vector is given by

$$\dot{\underline{\epsilon}} = \underset{\sim}{B}\,\dot{\underline{P}} \tag{2.33}$$

where $\underset{\sim}{B}$ is the strain rate matrix, given by

$$\underset{\sim}{B} = \begin{bmatrix} S_1'' & S_2'' & 0 & 0 & 0 & S_3'' & S_4'' & 0 & 0 & 0 \\ 0 & 0 & S_1'' & S_2'' & 0 & 0 & 0 & s_3'' & S_4'' & 0 \\ 2J_1 & 2J_2 & 2J_3 & 2J_4 & J_5 & 2J_6 & 2J_7 & 2J_8 & 2J_9 & J_{10} \end{bmatrix} \tag{2.34}$$

Substituting (2.20) and (2.33) into the energy equation, Equation (2.19), gives

$$\dot{\underline{P}}^T\underline{F} + \int_o^\ell [\dot{\underline{P}}^T\underset{\sim}{S}^T\,\underline{b}]\,dz = \int_o^\ell [\dot{\underline{P}}^T\underset{\sim}{B}^T\,\underline{\sigma}]\,dz\ ,$$

which can be written

$$\dot{\underline{P}}^T\,[\underline{F} + \int_o^\ell \underset{\sim}{S}^T\underline{b}\,dz - \int_o^\ell \underset{\sim}{B}^T\,\underline{\sigma}\,dz] = \underline{0} \tag{2.35}$$

By the principle of virtual work, $\dot{\underline{P}}$ can be varied independently of the term in brackets in (2.35). This implies that the term in brackets must equal zero. Therefore, we have

$$\underline{F} = \int_o^\ell \underset{\sim}{B}^T\,\underline{\sigma}\,dz - \int_o^\ell \underset{\sim}{S}^T\,\underline{b}\,dz\ . \tag{2.36}$$

This equation relates the nodal forces on the element to the stresses which exist inside the element.

Our goal here is to relate the nodal forces $\underline{F}$ to the nodal displacements $\underline{P}$. The usual procedure for accomplishing this is to first relate the stress in Equation (2.36) to the strain using the material stress-strain relation, and then relate the strain to the nodal displacements using Equation (2.29). However, as is shown in Section III, the constitutive equation (stress-strain relation) is incremental and of the form

$$\Delta \underline{\sigma} = \underset{\sim}{D}\, \Delta \underline{\varepsilon} + \underline{E} \tag{2.37}$$

where a Δ indicates increment and $\underset{\sim}{D}$ and $\underline{E}$ are matrices which do not depend upon either $\Delta \underline{\sigma}$ or $\Delta \underline{\varepsilon}$. To use Equation (2.37) in (2.36) we must also put (2.36) in incremental form. To do this, expand (2.36) in a Taylor series and retain only first-order terms to obtain

$$\underline{F}_o + \Delta \underline{F} = \int_o^{\ell} \underset{\sim o}{B}^T \underline{\sigma}_o \, dz + \int_o^{\ell} \underset{\sim o}{B}^T \Delta \underline{\sigma} \, dz + \int_o^{\ell} \Delta \underset{\sim}{B}^T \underline{\sigma}_o \, dz$$

$$- \int_o^{\ell} \underset{\sim}{S}^T \underline{b}_o \, dz - \int_o^{\ell} \underset{\sim}{S}^T \Delta \underline{b} \, dz$$

which, after re-arranging becomes

$$\Delta \underline{F} = \int_o^{\ell} \underset{\sim o}{B}^T \Delta \underline{\sigma} \, dz + \int_o^{\ell} \Delta \underset{\sim}{B}^T \underline{\sigma}_o \, dz - \int_o^{\ell} \underset{\sim}{S}^T \Delta \underline{b} \, dz + \underline{C} \tag{2.38}$$

where

$$\underline{C} = \int_o^{\ell} \underset{\sim o}{B}^T \underline{\sigma}_o \, dz - \int_o^{\ell} \underset{\sim}{S}^T \underline{b}_o \, dz - \underline{F}_o \quad . \tag{2.39}$$

A zero subscript indicates that the quantity is evaluated at the start of the increment. The $\underline{C}$ vector can be interpreted as a force correction term which corrects for any force imbalance at the beginning of a time step.

The second integral on the right-hand side of (2.38) can be written

$$\int_o^{\ell} \Delta \underset{\sim}{B}^T \underline{\sigma}_o \, dz = \underset{\sim \sigma}{K} \Delta \underline{P} \tag{2.40}$$

where

$$\underset{\sim \sigma}{K} = (2/\ell)\, \underset{\sim}{A} \int_o^{\ell} T_o \, dz \tag{2.41}$$

where T_o is the axial force, and where $\underset{\sim}{A}$ is defined by (2.24). The matrix $\underset{\sim \sigma}{K}$ is called the geometric, or initial stress, matrix.

We now assume that the incremental constitutive equation of the material is known in the form*

$$\Delta\underline{\sigma} = \underset{\sim}{D}\,\Delta\underline{\varepsilon} + \underline{E} \,. \tag{2.42}$$

When (2.42) is substituted into the first integral on the right-hand side of (2.38), that term becomes

$$\int_o^\ell \underset{\sim o}{B}^T \Delta\underline{\sigma}\, dz = \int_o^\ell \underset{\sim o}{B}^T \underset{\sim}{D}\, \Delta\underline{\varepsilon}\, dz + \int_o^\ell \underset{\sim o}{B}^T \underline{E}\, dz \quad . \tag{2.43}$$

From Equation (2.33) we obtain

$$\Delta\underline{\varepsilon} = \underset{\sim o}{B}\, \Delta\underline{P} \quad . \tag{2.44}$$

When (2.44) is substituted into (2.43) we obtain

$$\int_o^\ell \underset{\sim o}{B}^T \Delta\underline{\sigma}\, dz = \{\int_o^\ell \underset{\sim o}{B}^T \underset{\sim}{D}\, \underset{\sim o}{B}\, dz\}\, \Delta\underline{P} + \int_o^\ell \underset{\sim o}{B}^T \underline{E}\, dz \tag{2.45}$$

or

$$\int_o^\ell \underset{\sim o}{B}^T \Delta\underline{\sigma}\, dz = \underset{\sim}{\overline{K}}\, \Delta\underline{P} + \int_o^\ell \underset{\sim o}{B}^T \underline{E}\, dz \tag{2.46}$$

where

$$\underset{\sim}{\overline{K}} = \int_o^\ell \underset{\sim o}{B}^T \underset{\sim}{D}\, \underset{\sim o}{B}\, dz \quad . \tag{2.47}$$

The matrix $\underset{\sim}{\overline{K}}$ is called the initial displacement matrix or large displacement matrix [6].

When (2.46) and (2.40) are substituted into (2.38), we obtain

$$\Delta\underline{F} = (\underset{\sim}{\overline{K}} + \underset{\sim\sigma}{K})\, \Delta\underline{P} + \int_o^\ell \underset{\sim o}{B}^T \underline{E}\, dz - \int_o^\ell \underset{\sim}{S}^T \Delta\underline{b}\, dz + \underline{C} \tag{2.48}$$

---

* The calculation of $\underset{\sim}{D}$ and $\underline{E}$ will be described in Section III.

or

$$\Delta \underline{F} = \underset{\sim}{K}\, \Delta \underline{P} + \underline{H} \quad . \tag{2.49}$$

This set of ten equations represents the element incremental stiffness equations. The matrix $\underset{\sim}{K}$ is the incremental stiffness matrix and the vector $\underline{H}$ is the nodal force increment which would occur even if there were no increment in the nodal displacements.

The integrals appearing in Equation (2.48) and the integrals which define $\underset{\sim}{\overline{K}}$, $\underset{\sim}{K}_\sigma$ and $\underline{C}$ are all easily evaluated using Gaussian quadrature. The stiffness matrix $\underset{\sim}{K}$ and force vector $\underline{H}$ are calculated for each element starting with the first element. Because the stiffness matrix is symmetric, not all components need to be calculated.

C. The Global Stiffness Equations - The Assembly Procedure

It will be shown in this section that the global, or structure, stiffness equations can be written in the form

$$\underset{\sim}{K}_G\, \Delta \underline{P} + \underline{H}_G = \Delta \underline{F}_G \tag{2.50}$$

where $\underset{\sim}{K}_G$ is the symmetric global stiffness matrix, $\Delta \underline{P}$ is the nodal parameter increment vector for the entire structure, $\underline{H}_G$ is an initial force increment term, and $\Delta \underline{F}_G$ is the net external force increment on the nodes. As each element stiffness matrix and force vector are generated, they are used to construct the global stiffness matrix and global force vector.

Within each element, the nodal parameters are numbered from 1 to 10. The element parameters are also numbered according to a global numbering system. In the global numbering system, the parameters of the first element correspond to global parameters 1 through 10. The 10 parameters of the second element correspond to global parameters 6 through 15, etc.

Suppose now that the stiffness matrix and the force vector for the first element have been determined. The stiffness equations for that element will be of the form

$$[\,K^1\,]\,[\,\Delta P\,] + [\,H^1\,] = [\,\Delta F^1\,] \tag{2.51}$$

where K^1 is a 10x10 matrix and the components of $\Delta\underline{P}$, $\underline{H}^1$ and $\Delta\underline{F}^1$ are numbered from 1 to 10 corresponding to the local numbering system. We can now express the above set of equations using the global numbering system to get

$$\left[\begin{array}{c|ccc} & & & \\ \underset{\sim}{K}^1 & & 0 & \\ & & & \\ \hline & & & \\ 0 & & 0 & \end{array}\right]\left[\begin{array}{c} \Delta P_1 \\ \vdots \\ \Delta P_{10} \\ \hline \Delta P_{11} \\ \vdots \\ \Delta P_{5N} \end{array}\right] + \left[\begin{array}{c} H_1^1 \\ \vdots \\ H_{10}^1 \\ \hline \\ 0 \end{array}\right] = \left[\begin{array}{c} \Delta F_1^1 \\ \vdots \\ \Delta F_{10}^1 \\ \hline \\ 0 \end{array}\right] . \tag{2.52}$$

Equation (2.52) says exactly the same thing as Equation (2.51); the only difference is that the parameters have now been assigned their global numbers, which for the first element, are identical to the local numbers.

Now consider element number 2. The element stiffness equations will again be of the form

$$[\,K^2\,]\,[\,\Delta P\,] + [\,H^2\,] = [\,\Delta F^2\,] \ , \tag{2.53}$$

but now, the parameters which are labeled 1 through 10 locally will be labeled 6 through 15 in the global system. Therefore, in the global system, Equation (2.53) becomes

$$\begin{bmatrix} 0 & 0 & \\ & \underset{\sim}{K}^2 & 0 \\ 0 & 0 & 0 \end{bmatrix} \begin{bmatrix} \\ \Delta P_6 \\ \\ \Delta P_{15} \\ \\ \\ \Delta P_{5N} \end{bmatrix} + \begin{bmatrix} 0 \\ H_6^2 \\ \\ H_{15}^2 \\ \\ 0 \end{bmatrix} = \begin{bmatrix} 0 \\ \Delta F_6^2 \\ \\ \Delta F_{15}^2 \\ \\ 0 \end{bmatrix} \qquad (2.54)$$

Equations similar to (2.52) and (2.54) could be written for all of the elements. The objective is to solve for the net external force acting on the nodes. The forces $\underline{F}^i$ given by equations such as (2.52) and (2.54) are the forces exerted on the element i at its nodes; thus, the forces $\underline{F}^i$ can also be interpreted as the negatives of the forces exerted on the nodes by the elements. If the node is to be in equilibrium, the external forces acting on the node must be equal to the sum of the negatives of all other forces acting on the node. Therefore the global stiffness equations are obtained by simply adding together all of the element stiffness equations written in global form. For a structure with five elements, this will produce a matrix stiffness equation in the form:

$$\begin{bmatrix} \underset{\sim}{K}_1 & & & & \\ & \underset{\sim}{K}_2 & & 0 & \\ & & \underset{\sim}{K}_3 & & \\ & & & \underset{\sim}{K}_4 & \\ 0 & & & & \underset{\sim}{K}_5 \end{bmatrix} \begin{bmatrix} \Delta P_1 \\ \\ \Delta P_{10} \\ \Delta P_{11} \\ \\ \\ \Delta P_{30} \end{bmatrix} + \begin{bmatrix} H_1 \\ \\ H_{10} \\ \\ \\ \\ H_{30} \end{bmatrix} = \begin{bmatrix} \Delta F_1 \\ \\ \Delta F_{10} \\ \\ \\ \\ \Delta F_{30} \end{bmatrix}$$

or

$$\underset{\sim}{K}_G \, \underline{\Delta P} + \underline{H}_G = \underline{\Delta F}_G \, . \qquad (2.55)$$

Thus, in setting up the $\underset{\sim}{K}_G$ and $\underline{H}_G$ matrices there will be an overlap of five parameters between elements. The $\underset{\sim}{K}_G$ matrix will be symmetric and have a half-bandwidth of 10. This matrix can be stored in a compressed form; the exact form will depend upon the equation solver used.

D. Boundary Conditions

Equation (2.55) is a relation between the nodal force increments and the nodal displacement increments. To specify a particular type of support or loading on the structure, some of the displacement increments may be specified, some of the force increments may be specified, or a relation between some of the force increments and displacement increments may be specified. Figure 3 shows a representation of the various types of boundary conditions which can be used to model the rod supports. For simplicity only the x-z plane is shown. At support number 1 force-type* boundary conditions are assumed for all degrees of freedom, while at support number 2 displacement boundary conditions are applied. At support number 3, flexible boundary conditions are applied to all degrees of freedom and a support axial displacement is also assumed. At support number 4 a frictional boundary condition is applied in the axial direction, a displacement boundary condition is applied in the x-direction, and a rotational force (i.e. a moment) boundary condition is applied in the x-z plane.

We now consider how Equation (2.55) can be modified so as to enforce the various boundary condition types.

(a) Specified Force Boundary Condition

This is the easiest type to enforce. The force increment is merely substituted into the appropriate row of the $\Delta\underline{F}_G$ matrix. All other components of $\Delta\underline{F}_G$ are initially zero.

---

* "Force" and "displacement" are used in a generalized sense here. They may refer to a moment and an angle for some of the degrees of freedom.

(b) Specified Displacement Boundary Conditions

In this case, one of the equations of (2.55) is replaced by an equation which simply states that the appropriate displacement increment equals the specified value. If the ith displacement increment is specified, a simple way to do this is to multiply $(K_G)_{ii}$ by a very large number, say L. Next set $(H_G)_i$ to zero and set $(\Delta F_G)_i$ to L x (specified displacement increment). Numerically, this has the effect of setting up an equation of the form

$$L \times \Delta P_i = L \times (\text{Specified } \Delta P_i)$$

or

$$\Delta P_i = (\text{Specified } \Delta P_i)$$

since the other terms in the equation will be numerically negligible.

(c) Flexible Boundary Conditions

With this type of boundary condition there will be a relation of the form

$$\Delta F_i = C_i \Delta P_i + (\Delta F_i)_o \qquad (2.56)$$

where C_i may depend upon P_i and F_i is the force increment exerted on the flexible element. This equation can be regarded as an element stiffness equation of a flexible element joined only to the variable i. Therefore it can simply be added to the global stiffness equations. To do this, add C_i to $(K_G)_{ii}$ and add $(\Delta F_i)_o$ to $(H_G)_i$.

(d) Frictional Boundary Conditions

A frictional boundary condition can be either a displacement or a force boundary condition, depending on the magnitude of the particular nodal force. If the force is less than the slippage force, the boundary condition specifies that the displacement increment is zero. If the force exceeds the frictional force, the calculation is re-done and the nodal force

is set equal to the slippage force. The frictional force must always oppose the motion of the rod. If the displacement increment of the rod is ever in the same direction as the frictional force, the boundary condition is changed to again set the displacement increment to zero and the calculation is re-done. Several iterations may be required before the right combination of boundary conditions is found. To reduce the number of computations involved in this iterative loop, the frictional boundary condition should be inserted last. Before inserting the frictional boundary conditions, the matrices $\underset{\sim}{K}_G$, $\underline{H}_G$ and $\Delta\underline{F}_G$ have been modified by insertion of all other boundary conditions. Denote these modified matrices by $\hat{\underset{\sim}{K}}_G$, $\hat{\underline{H}}_G$ and $\Delta\hat{\underline{F}}_G$. These matrices can be saved so that new frictional boundary conditions can be easily tried if a guess turns out to be wrong. In addition, these matrices can be used to evaluate the nodal forces at nodes which are assumed not to slip. This procedure is discussed more fully in the next section. For simplicity, it is assumed that frictional boundary conditions apply only to axial displacements.

E. Calculation of the Nodal Displacement, Stress, and Strain Increments

The nodal displacement increments can be obtained by solving the equation

$$\underset{\sim}{K}^*_G \, \Delta\underline{P} = (\Delta\underline{F}^*_G - \underline{H}^*_G) \tag{2.57}$$

where a * denotes that the quantities have been modified by insertion of all boundary conditions. Equation (2.57) can be solved for $\Delta\underline{P}$ using a library subroutine for solving equations with a banded, symmetric, positive-definite coefficient matrix.

If the problem involves frictional boundary conditions, the assumptions used to formulate the boundary conditions must be checked at this time. If the slippage force has been applied to any of the nodes, the axial displacement increment must be opposite the direction of the applied loads; otherwise, the assumptions must be changed and the calculation re-done. Next, the axial nodal forces are calculated from the equation

$$\Delta\underline{F}_G = \hat{\underset{\sim}{K}}_G \, \Delta\underline{P} + \hat{\underline{H}}_G$$

where $\hat{\underset{\sim}{K}}_G$ and $\hat{\underset{\sim}{H}}_G$ are the matrices which were saved before insertion of the frictional boundary conditions. If the axial forces are such that nodes which were assumed not to slip must have slipped, the calculation must be re-done. This process is repeated until the correct boundary conditions are obtained.

After the nodal displacement increments have been calculated, the stress and strain increments at the element Gauss points can be calculated. The strain increments are given by

$$\Delta \underline{\epsilon} = \underset{\sim}{B}\, \Delta \underline{P} \tag{2.58}$$

After the strain increments have been calculated, the stress increments are easily calculated using the constitutive equation (2.42).

The procedure described above represents a single time-step iteration. It has been found that a significant improvement in the time integration accuracy can be achieved by using two iterations per time step. With this method, the first iteration is performed as described above and the average values during the time step of the nodal displacements are approximately calculated. The stiffness equations for the rod are re-calculated using these average values and the time step is then re-taken. This procedure is similar to the second-order Runge-Kutta method used in the solution of ordinary differential equations. Because the rod constitutive equations are not re-evaluated for the second iteration, the computer run time will not be significantly increased by using two iterations rather than one.

III. The Constitutive Equation of the Fuel Rod

The purpose of this section is to formulate the fuel rod constitutive equation in the form

$$\Delta \underline{\sigma} = \underset{\sim}{D}\, \Delta \underline{\epsilon} + \underline{E}\ . \tag{3.1}$$

The constitutive equation for fuel rods containing either single-zone or duplex fuel is modeled using a method which is essentially the same as the method originally formulated in Reference [1]. The fuel-cladding interaction model has been slightly modified and has been extended to account for fuel-fuel interaction in duplex fuels.

The formulate Equation (3.1), the assumption is made that the effects of bending do not significantly change the incremental stress-strain relations associated with the axisymmetric deformations of the rod. Experience has shown that this is a valid assumption because the stress variations due to bending are usually small compared to the axisymmetric stresses. This assumption makes it possible to assign incremental stress-strain relations using an axisymmetric fuel element analysis program such as CYGRO [4]. Material properties and material constitutive relations used in the bowing analysis are identical to those used in CYGRO.

A. The Ring Constitutive Equations

The CYGRO computer program calculates the cylindrically symmetric stresses and deformations in a fuel rod by dividing the rod cross-section into a set of finite elements in the form of concentric rings as shown in Figure 4. The stress within each ring is assumed to be constant. To formulate the constitutive equation (3.1), it is assumed that the stresses due to bending and support constraints can be regarded as a perturbation of the CYGRO-calculated axisymmetric stress state.

In terms of the perturbational stress in the z direction, S_z, the total strain rate in the z direction, $\dot{\varepsilon}^t_z$, can be approximated by

$$\dot{\varepsilon}^t_z = \left(\frac{\partial \dot{\varepsilon}_{cz}}{\partial S_z}\right) S_z + \left(\frac{\partial \dot{\varepsilon}_{ez}}{\partial S_z}\right) \dot{S}_z + \dot{\varepsilon}_{iz} \qquad (3.2)$$

where $\dot{\varepsilon}_{cz}$ is the creep strain rate, $\dot{\varepsilon}_{ez}$ is the elastic strain rate, and $\dot{\varepsilon}_{iz}$ is the induced strain rate. The induced strain rate is the strain rate which would occur even if S_z and $\dot{S}_z$ were zero and accounts for effects such as thermal expansion, flux-induced stress-free growth, and the CYGRO-calculated axial strain rate. The first partial derivative in (3.2) is the zz component of the creep compliance matrix and is calculated from the creep constitutive equations. The second partial derivative in (3.2) is just the zz component of the elastic compliance matrix. These quantities are calculated in CYGRO and written into a data file.

If it is assumed that plane cross-sections of the rod remain plane during bending, the total axial strain rate in one of the CYGRO rings can be written

$$\dot{\varepsilon}_z^t = \dot{\varepsilon} + \dot{\kappa}^x \, r \cos\theta + \dot{\kappa}^y \, r \sin\theta \tag{3.3}$$

where κ_x and κ_y are the curvatures of the fuel rod in the x-z and y-z planes respectively, $\dot{\varepsilon}$ is a uniform axial strain, and r and θ are polar coordinates in the plane of the cross section with r=0 at the center of the rod and θ=0 along the x-axis. This arrangement is shown in Figure 5. Combining Equations (3.2) and (3.3), we obtain

$$\frac{S_z}{V_k} + \frac{\dot{S}_z}{E_k} = \dot{\kappa}^x \, r \cos\theta + \dot{\kappa}^y \, r \sin\theta + (\dot{\varepsilon} - \dot{\varepsilon}_{iz}) \tag{3.4}$$

where the notation

$$\frac{1}{V_K} = \left(\frac{\partial \dot{\varepsilon}_{cz}}{\partial S_z}\right)_k, \quad \frac{1}{E_k} = \left(\frac{\partial \dot{\varepsilon}_{ez}}{\partial \dot{S}_z}\right)_k$$

has been used. Note that the constants V_k and E_k are obtained from the CYGRO data file. The k subscript denotes that the quantity is for the kth CYGRO ring. We now make the assumption that the induced strain rate can be written in the form

$$\dot{\varepsilon}_{iz} = \dot{\varepsilon}^i + \dot{\kappa}_k^{xi} \, r \cos\theta + \dot{\kappa}_k^{yi} \, r \sin\theta \tag{3.5}$$

where $\dot{\varepsilon}^i$ is the uniform axial strain rate calculated by CYGRO and where κ_k^{xi} and κ_k^{yi} are the induced curvatures for ring k. This is equivalent to the assumption that if only induced axial strains were present, plane cross sections of the rod would remain plane. The induced curvatures are the moment-free curvatures caused by non-axisymmetric environmental and structural factors such as transverse temperature gradients, transverse fast-neutron flux gradients, and cladding wall thickness eccentricity. The calculation of these curvatures is discussed in Section IV.

Substitution of Equation (3.5) into (3.4) gives

$$\frac{S_z}{V_k} + \frac{\dot{S}_z}{E_k} = (\dot{\kappa}^x - \dot{\kappa}^{xi}_k)\, r \cos\Theta + (\dot{\kappa}^y - \dot{\kappa}^{yi}_k)\, r \sin\Theta + (\dot{\varepsilon} - \dot{\varepsilon}^i) \ . \qquad (3.6)$$

Integrating (3.6) over the ring cross-section gives

$$\frac{T_k}{V_k} + \frac{\dot{T}_k}{E_k} = (\dot{\varepsilon} - \dot{\varepsilon}^i)\, A_k \qquad (3.7)$$

where A_k is the ring cross-sectional area given by

$$A_k = \pi\, (r_{k0}^2 - r_{kI}^2)$$

and where T_k is the axial force on the ring, given by

$$T_k = \int_{A_k} S_z \, dA \ .$$

Multiplying (3.6) by r cos Θ and integrating gives

$$\frac{M_k^x}{V_k} + \frac{\dot{M}_k^x}{E_k} = (\dot{\kappa}^x - \dot{\kappa}^{xi}_k) I_k \qquad (3.8)$$

where I_k is the moment of inertia of the ring cross-sectional area about the y axis, given by

$$I_k = (\pi/4)\, (r_{ko}^4 - r_{ki}^4) \qquad (3.9)$$

and M_k^x is the x-component of the moment acting on ring k, given by

$$M_k^x = \int_{A_K} r\, S_z \cos\Theta \, dA \ .$$

Similarly, multiplying (3.6) by r sin Θ and integrating gives

$$\frac{M_k^y}{V_k} + \frac{\dot{M}_k^y}{E_k} = (\dot{\kappa}^y - \dot{\kappa}_k^{yi}) I_k \tag{3.10}$$

where M_k^y is the moment acting in the y-z plane, given by

$$M_k^y = \int_{A_K} r\, S_z \sin\Theta \, dA ,$$

and where I_k is again given by (3.9). Equations (3.7), (3.8), and (3.10) are differential equations which characterize the behavior of a single ring. Because the rod deflections and slopes are assumed to be small, the curvatures κ^x and κ^y can be approximated by

$$\left.\begin{aligned} \kappa^x &= \frac{d^2u}{dz^2} \\ \kappa^y &= \frac{d^2v}{dz^2} \end{aligned}\right\} \tag{3.11}$$

To obtain the incremental equations, Equations (3.7), (3.8), and (3.10) are multiplied by a time increment Δt to obtain

$$\Delta M_k^x = a_k^x \Delta\kappa^x + b_k^x \tag{3.12}$$

$$\Delta M_k^y = a_k^y \Delta\kappa^y + b_k^y \tag{3.13}$$

$$\Delta T_k = a_k^z \Delta\epsilon + b_k^z \tag{3.14}$$

where

$$a_k^x = E_k\ I_k \tag{3.15}$$

$$a_k^y = E_k\ I_k \tag{3.16}$$

$$a_k^z = E_k\ A_k \tag{3.17}$$

$$b_k^x = -\ E_k(I_k\ \dot{\kappa}_k^{xi} + M_k^x/V_k)\ \Delta t \tag{3.18}$$

$$b_k^y = -\ E_k(I_k\ \dot{\kappa}_k^{yi} + M_k^y/V_k)\ \Delta t \tag{3.19}$$

$$b_k^z = -\ E_k(A_k\ \dot{\varepsilon}^i + T_k/V_k)\ \Delta t \tag{3.20}$$

Once the curvature and axial strain increments are obtained using the finite element procedure, the moment and axial force increments can be back calculated using Equations (3.12), (3.13), and (3.14). The beginning-of-time-step values of the axial force and moments used in Equations (3.18), (3.19), and (3.20) are obtained by keeping track of the sum of the increments of these quantities.

B. The Fuel and Cladding Constitutive Equations

The total moment or axial force acting in either the cladding or one of the fuel zones is equal to the sum of the moments or axial forces in the rings contained in the cladding or fuel zone. Thus, the fuel zone or cladding constitutive equations can be obtained by summing the ring constitutive equations to obtain

$$\left.\begin{aligned} \Delta T_{fi} &= A_{fi}^z\ \Delta\varepsilon_{fi} + B_{fi}^z \\ \Delta M_{fi}^x &= A_{fi}^x\ \Delta\kappa_{fi}^x + B_{fi}^x \\ \Delta M_{fi}^y &= A_{fi}^y\ \Delta\kappa_{fi}^y + B_{fi}^y\ , \end{aligned}\right\}\ i = 1,2 \tag{3.21}$$

and

$$\left.\begin{aligned} \Delta T_c &= A_c^z\ \Delta\varepsilon_c + B_c^z \\ \Delta M_c^x &= A_c^x\ \Delta\kappa_c^x + B_c^x \\ \Delta M_c^y &= A_c^y\ \Delta\kappa_c^y + B_c^y \end{aligned}\right\} \tag{3.22}$$

where the f1, f2 and c subscripts denote "fuel zone 1", "fuel zone 2", and "cladding" respectively. It will be assumed that fuel zone 1 is the inner fuel zone and fuel zone 2 is the outer fuel zone. If the fuel is single-zone, then only fuel zone 2 is present. In the above equations the A's and B's are given by

$$\left.\begin{aligned} A^z_{fi} &= \sum_{fi} a^z_k \quad , \quad B^z_{fi} = \sum_{fi} b^z_k \\ A^x_{fi} &= A^y_{fi} = \sum_{fi} a^x_k \\ B^x_{fi} &= \sum_{fi} b^x_k \quad , \quad B^y_{fi} = \sum_{fi} b^y_k \end{aligned}\right\} \quad i = 1,2$$

and

$$A^z_c = \sum_c a^z_k \quad , \quad B^z_c = \sum_c b^z_k$$

$$A^x_c = A^y_c = \sum_c a^x_k$$

$$B^x_c = \sum_c b^x_k \quad , \quad B^y_c = \sum_c b^y_k$$

where the notation $\sum_{fi}$ and $\sum_{c}$ indicates that the summation is over the rings in either fuel zone i or the cladding. If a fuel ring is cracked on a plane perpendicular to the z-direction, the constant V_k is set to a very small number for that ring. This has the effect of making the ring very weak, thereby making the axial forces and moments in the ring go to zero.

C. Fuel-Cladding Interaction Model

The bending interaction of the fuel and cladding is assumed to take place through a coupling element which is assumed to have an elastic bending stiffness G_a given by

$$G_a = \left[\frac{\eta_a}{1-\eta_a}\right] \sum_{f2} E_k I_k, \quad 0 \leq \eta_a < 1$$

and a bending viscosity given by

$$W_a = \beta_a \sum_{f2} V_k I_k, \quad \beta_a \geq 0$$

where η and β are constants and where, again, cracked rings are ignored in the summations. The constants η_a and β_a are supplied as input to the bowing analysis program. The constitutive equations for the interaction element will be

$$\frac{M_a^x}{W_a} + \frac{\dot{M}_a^x}{G_a} = \dot{\kappa}_a^x$$

$$\frac{M_a^y}{W_a} + \frac{\dot{M}_a^y}{G_a} = \dot{\kappa}_a^y \quad .$$

and the incremental forms of these equations will be

$$\Delta M_a^x = A_a^x \Delta\kappa_a^x + B_a^x \tag{3.23}$$

$$\Delta M_a^y = A_a^y \Delta\kappa_a^y + B_a^y \tag{3.24}$$

where

$$A_a^x = A_a^y = G_a$$

$$B_a^x = -(G_a M_a^x / W_a)\,\Delta t$$

$$B_a^y = -(G_a M_a^y / W_a)\,\Delta t$$

A similar type of interaction element is used to account for the bending interaction of the two fuel zones. The bending stiffness and viscosity for this element is defined by

$$\left.\begin{aligned} G_b &= \left[\frac{\eta_b}{1-\eta_b}\right] \sum_{fl} E_k I_k \\ \text{and} \\ W_b &= \beta_b \sum_{fl} V_k I_k \quad . \end{aligned}\right\} \qquad (3.25)$$

Again, η_b and β_b are user-supplied constants. The incremental constitutive equations for the fuel-fuel interaction element will be

$$\Delta M_b^x = A_b^x \Delta\kappa_b^x + B_b^x \qquad (3.26)$$

$$\Delta M_a^y = A_b^y \Delta\kappa_b^y + B_b^y \qquad (3.27)$$

where

$$\left.\begin{aligned} A_b^x &= A_b^y = G_b \\ B_b^x &= -(G_b M_b^x / W_b)\,\Delta t \\ B_b^y &= -(G_b M_b^y / W_b)\,\Delta t \end{aligned}\right\} \qquad (3.28)$$

If there is only one fuel zone, the constitutive equation for the fuel-fuel interaction element will not be calculated.

The form of the rod constitutive equation (3.1) will depend upon the interaction state of the fuel zones and the cladding. For fuel rods with duplex fuel, there are four possibilities given by:

(1) no fuel-fuel or fuel-cladding interaction,

(2) fuel-cladding interaction only,

(3) fuel-fuel interaction only, and

(4) fuel-fuel and fuel-cladding interaction.

For single-zone fuel, it is assumed that only states (1) and (2) are possible. The constitutive equations corresponding to these four states are given below.

(1) No fuel-fuel or fuel-clad interaction

The constitutive equations of the fuel rod will be

$$\left.\begin{aligned} \Delta M^x &= A_c^x \, \Delta\kappa^x + B_c^x \\ \Delta M^y &= A_c^y \, \Delta\kappa^y + B_c^y \\ \Delta T &= A_c^z \, \Delta\epsilon + B_c^z \quad . \end{aligned}\right\} \tag{3.29}$$

The axial strain and curvature increments in fuel zone 2 will be

$$\left.\begin{aligned} \Delta\kappa_{f2}^x &= -(B_{f2}^x / A_{f2}^x) \\ \Delta\kappa_{f2}^y &= -(B_{f2}^y / A_{f2}^y) \\ \Delta\epsilon_{f2} &= -(B_{f2}^z / A_{f2}^z) \quad . \end{aligned}\right\} \tag{3.30}$$

If the rod has duplex fuel, the strain increments in zone 1 will be

$$\left.\begin{aligned} \Delta\kappa_{f1}^x &= -(B_{f1}^x / A_{f1}^x) \\ \Delta\kappa_{f1}^y &= -(B_{f1}^y / A_{f1}^y) \\ \Delta\epsilon_{f1} &= -(B_{f1}^z / A_{f1}^z) \quad . \end{aligned}\right\} \tag{3.31}$$

(2) Fuel-cladding interaction only

In this case, the rod constitutive equation will be

$$\left.\begin{aligned} \Delta M^x &= \left[A_c^x + \frac{A_{f2}^x \, A_a^x}{A_{f2}^x + A_a^x}\right] \Delta\kappa^x + \left[B_c^x + \frac{B_{f2}^x \, A_a^x + B_a^x \, A_{f2}^x}{A_{f2}^x + A_a^x}\right] \\ \Delta M^y &= \left[A_c^y + \frac{A_{f2}^y \, A_a^y}{A_{f2}^y + A_a^y}\right] \Delta\kappa^y + \left[B_c^y + \frac{B_{f2}^y \, A_a^y + B_a^y \, A_{f2}^y}{A_{f2}^y + A_a^y}\right] \\ \Delta T &= \left[A_{f2}^z + A_c^z\right] \Delta\epsilon + \left[B_{f2}^z + B_c^z\right] \quad . \end{aligned}\right\} \tag{3.32}$$

The strain increments in fuel zone 2 will be

$$\left.\begin{aligned} \Delta\kappa^x_{f2} &= \left[\frac{A^x_a}{A^x_a + A^x_{f2}}\right] \Delta\kappa^x - \left[\frac{B^x_{f2} - B^x_a}{A^x_a + A^x_{f2}}\right] \\ \Delta\kappa^y_{f2} &= \left[\frac{A^y_a}{A^y_a + A^y_{f2}}\right] \Delta\kappa^y - \left[\frac{B^y_{f2} - B^y_a}{A^y_a + A^y_{f2}}\right] \\ \Delta\varepsilon_{f2} &= \Delta\varepsilon \end{aligned}\right\} \qquad (3.33)$$

and the curvature increments in the fuel-cladding interaction element will be

$$\left.\begin{aligned} \Delta\kappa^x_a &= \Delta\kappa^x - \Delta\kappa^x_{f2} \\ \Delta\kappa^y_a &= \Delta\kappa^y - \Delta\kappa^y_{f2} \quad . \end{aligned}\right\} \qquad (3.34)$$

If the fuel is dual zone, the strain increments in zone 1 will again be given by Equations (3.31).

(3) Fuel-fuel interaction only (Duplex fuel only)

The fuel rod constitutive equation will be

$$\left.\begin{aligned} \Delta M^x &= A^x_c \Delta\kappa^x + B^x_c \\ \Delta M^y &= A^y_c \Delta\kappa^y + B^y_c \\ \Delta T &= A^z_c \Delta\varepsilon + B^z_c \quad . \end{aligned}\right\} \qquad (3.35)$$

The strain increments in fuel zone 2 will be given by

$$\left.\begin{aligned} \Delta\kappa^x_{f2} &= -B^x_2/A^x_2 \\ \Delta\kappa^y_{f2} &= -B^y_2/A^y_2 \\ \Delta\varepsilon_{f2} &= -(B^z_{f2} + B^z_{f1})/(A^z_{f2} + A^z_{f1}) \end{aligned}\right\} \qquad (3.36)$$

where

$$\left.\begin{aligned} A_2^x &= A_{f2}^x + \frac{A_{f1}^x\, A_b^x}{A_{f1}^x + A_b^x} \\ A_2^y &= A_{f2}^y + \frac{A_{f1}^y\, A_b^y}{A_{f1}^y + A_b^y} \\ B_2^x &= B_{f2}^x + \frac{B_{f1}^x\, A_b^x + B_b^x\, A_{f1}^x}{A_{f1}^x + A_b^x} \end{aligned}\right\} \qquad (3.37)$$

and

$$B_2^y = B_{f2}^y + \frac{B_{f1}^y\, A_b^y + B_b^y\, A_{f1}^y}{A_{f1}^y + A_b^y} \quad .$$

The strain increments in fuel zone 1 will be

$$\left.\begin{aligned} \Delta\kappa_{f1}^x &= \left[\frac{A_b^x}{A_{f1}^x + A_b^x}\right] \Delta\kappa_{f2}^x + \left[\frac{B_b^x - B_{f1}^x}{A_{f1}^x + A_b^x}\right] \\ \Delta\kappa_{f1}^y &= \left[\frac{A_b^y}{A_{f1}^y + A_b^y}\right] \Delta\kappa_{f2}^y + \left[\frac{B_b^y - B_{f1}^y}{A_{f1}^y + A_b^y}\right] \end{aligned}\right\} \qquad (3.38)$$

$$\Delta\varepsilon_{f1} = \Delta\varepsilon_{f2} \quad .$$

The curvature increments in the fuel-fuel interaction element will be

$$\left.\begin{aligned} \Delta\kappa_b^x &= \Delta\kappa_{f2}^x - \Delta\kappa_{f1}^x \\ \Delta\kappa_b^y &= \Delta\kappa_{f2}^y - \Delta\kappa_{f1}^y \quad . \end{aligned}\right\} \qquad (3.39)$$

(4) Fuel-fuel and fuel-cladding interaction (Duplex fuel only)

The fuel rod constitutive equations will be

$$\Delta M^x = [A_c^x + \frac{A_a^x A_2^x}{A_a^x + A_2^x}] \Delta\kappa^x + [B_c^x + \frac{B_a^x A_2^x + B_2^x A_a^x}{A_a^x + A_2^x}]$$

$$\Delta M^y = [A_c^y + \frac{A_a^y A_2^y}{A_a^y + A_2^y}] \Delta\kappa^y + [B_c^y + \frac{B_a^y A_2^y + B_2^y A_a^y}{A_a^y + A_2^y}] \quad (3.40)$$

$$\Delta T = [A_{f1}^z + A_{f2}^z + A_c^z] \Delta\varepsilon + [B_{f1}^z + B_{f2}^z + B_c^z]$$

where A_2^x, A_2^y, B_2^x and B_2^y and B_2^y are defined by Equations (3.37). The strain increment in fuel zone 2 will be given by

$$\Delta\kappa_{f2}^x = [\frac{A_a^x}{A_a^x + A_2^x}] \Delta\kappa^x + [\frac{B_a^x - B_2^x}{A_a^x + A_2^x}]$$

$$\Delta\kappa_{f2}^y = [\frac{A_a^y}{A_a^y + A_2^y}] \Delta\kappa^y + [\frac{B_a^y - B_2^y}{A_a^y + A_2^y}] \quad (3.41)$$

$$\Delta\varepsilon_{f2} = \Delta\varepsilon$$

The strain increments in fuel zone 1 and the curvature increments in the fuel-fuel interaction element are given by Equations (3.38) and (3.39). The curvature increments in the fuel-cladding interaction element are given by Equation (3.34).

The fuel rod constitutive equations given above for the four possible interaction states are used whenever the interaction state is unchanged during the time step. If the interaction state changes during a time step, the elastic interaction between the fuel zones or cladding induces a jump in their curvatures at the beginning of the time step. In the constitutive equations for the fuel zones, the cladding, and the interaction elements, this curvature jump is accounted for by: (1) changing the initial curvature used in the constitutive equation, and (2) adding a jump term to the constitutive equation to correct the curvature increment. In addition, if interaction is established during a time step, the initial curvatures of the appropriate interaction element must be set. If there is a jump δ in the initial curvature of a fuel zone, cladding, or interaction element, the incremental constitutive equation becomes

$$\Delta M = A\,[\kappa_1 - (\kappa_o + \delta)] + B \tag{3.42}$$

The above equation can be re-written as

$$\Delta M = A\,\Delta\kappa + (B - A\delta)$$

$$= A\,\Delta\kappa + B_{new} \quad . \tag{3.43}$$

The above equation shows how the B term is modified when the jump in the initial curvature is known.

The curvature jumps are assumed to take place elastically and therefore the equations used to calculate the jumps will make use of the instantaneous elastic bending moduli of the fuel zones, the cladding, and the interaction elements. These elastic moduli are defined by

$$D_c = \sum_c E_k I_k \tag{3.44}$$

$$D_{f2} = \sum_{f2} E_k I_k \tag{3.45}$$

$$D_{f1} = \sum_{f1} E_k I_k \tag{3.46}$$

$$D_a = G_a = \left[\frac{\eta_a}{1 - \eta_a}\right] D_{f2} \tag{3.47}$$

$$D_b = G_b = \left[\frac{\eta_b}{1 - \eta_b}\right] D_{f1} \quad . \tag{3.48}$$

The equations will also make use of the parameters γ_a and γ_b, called the contact efficiencies, which represent the ratio of the observed curvature jumps to the curvature jumps which would be obtained if there were perfect interaction (i.e. elastic behavior and equal curvatures after interaction). Like η_a, β_a, η_b and β_b, these constants are determined experimentally and are provided as input to the bowing analysis computer program.

Because there are four possible interaction states in a fuel rod with duplex fuel, there will be twelve ways in which the state can change. In fuel rods containing single-zone fuel, only two of the twelve state changes are possible. The curvature jumps to be used for the twelve possible state changes will now be given. For convenience, a superscript ξ will denote either x- or y-direction terms. The interaction state changes can be visualized with the aid of the diagram shown below.

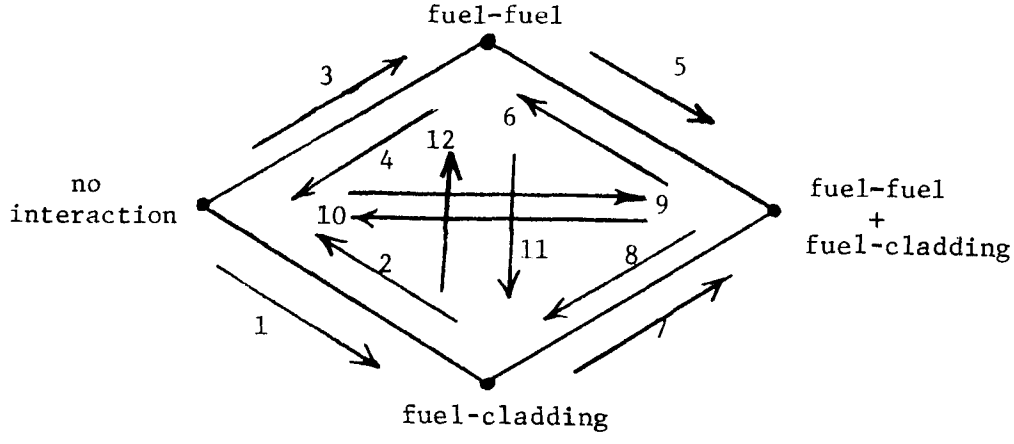

In what follows, expressions for the jump terms are given without derivation. These expressions can be derived by considering the displacement changes which occur in a set of inter-connected "springs" (representing the fuel zones, cladding, and interaction elements) when the connectivity of the system is suddenly changed. Such a system of inter-connected flexural springs can be visualized using an analogous set of linear springs (or elastic elements) connected as shown in Figure 8. In this diagram, force is analogous to moment and displacement is analogous to curvature.

(1) No interaction → fuel-cladding interaction

This type of state change can occur in fuel rods with either single-zone or dual-zone fuel. In this case

$$\left.\begin{aligned} \delta_c^{\xi} &= -\gamma_a \left[\frac{D_{f2}}{D_{f2} + D_c}\right] \left(\kappa_{c_o}^{\xi} - \kappa_{f2_o}^{\xi}\right) \\ \delta_{f2}^{\xi} &= \gamma_a \left[\frac{D_c}{D_{f2} + D_c}\right] \left(\kappa_{c_o}^{\xi} - \kappa_{f2_o}^{\xi}\right) \\ \delta_{f1}^{\xi} &= 0 \end{aligned}\right\} \qquad (3.49)$$

and

$$\kappa_{a_o}^{\xi} = \left\{1 - \gamma_a \left[\frac{\eta_a D_{f2} + D_c}{\eta_a (D_{f2} + D_c)}\right]\right\} \left(\kappa_o^{\xi} - \kappa_{f2_o}^{\xi}\right)$$

(2) Fuel-cladding interaction → no interaction

This type can also occur in fuel rods with either single-zone or dual-zone fuel.

$$\left.\begin{aligned} \delta_{f2}^{\xi} &= -(1/D_{f2}) \sum_{f2} M_k^{\xi} \\ \delta_c^{\xi} &= -(D_{f2}/D_c)\, \delta_{f2}^{\xi} \\ \delta_{f1}^{\xi} &= 0 \end{aligned}\right\} \qquad (3.50)$$

(3) No interaction → fuel-fuel interaction

$$\left.\begin{aligned}
\delta^{\xi}_{f2} &= -\gamma_b \left[\frac{D_{f1}}{D_{f1}+D_{f2}}\right] \left(\kappa^{\xi}_{f2_o} - \kappa^{\xi}_{f1_o}\right) \\
\delta^{\xi}_{f1} &= \gamma_b \left[\frac{D_{f2}}{D_{f1}+D_{f2}}\right] \left(\kappa^{\xi}_{f2_o} - \kappa^{\xi}_{f1_o}\right) \\
\delta^{\xi}_{c} &= 0 \\
\kappa^{\xi}_{b_o} &= \left\{1 - \gamma_b \left[\frac{\eta_b D_{f1} + D_{f2}}{\eta_b (D_{f1}+D_{f2})}\right]\right\} \left(\kappa^{\xi}_{f2_o} - \kappa^{\xi}_{f1_o}\right)
\end{aligned}\right\} \quad (3.51)$$

(4) Fuel-fuel interaction → no interaction

$$\left.\begin{aligned}
\delta^{\xi}_{f1} &= -(1/D_{f1}) \sum_{f1} M^{\xi}_{k} \\
\delta^{\xi}_{f2} &= -(D_{f1}/D_{f2})\, \delta^{\xi}_{f1} \\
\delta^{\xi}_{c} &= 0
\end{aligned}\right\} \quad (3.52)$$

(5) Fuel-fuel interaction → fuel-fuel and fuel-cladding interaction

$$\left.\begin{aligned}
\delta^{\xi}_{c} &= -\gamma_a \left(\frac{D_2}{D_2 + D_c}\right) \left(\kappa^{\xi}_{c_o} - \kappa^{\xi}_{f2_o}\right) \\
\delta^{\xi}_{f2} &= \gamma_a \left(\frac{D_c}{D_2 + D_c}\right) \left(\kappa^{\xi}_{c_o} - \kappa^{\xi}_{f2_o}\right) \\
\delta^{\xi}_{f1} &= \left(\frac{D_b}{D_{f1} + D_b}\right) \delta^{\xi}_{f2} \\
\delta^{\xi}_{b} &= \delta^{\xi}_{f2} - \delta^{\xi}_{f1} \\
\kappa^{\xi}_{a_o} &= \left\{1 - \gamma_a \left[\frac{\eta_a D_2 + D_c}{\eta_a (D_2 + D_c)}\right]\right\} \left(\kappa^{\xi}_{o} - \kappa^{\xi}_{f2_o}\right)
\end{aligned}\right\} \quad (3.53)$$

where D_2 is the fuel stiffness, given by

$$D_2 = D_{f2} + \frac{D_{f1} D_b}{D_{f1} + D_b} \quad .$$

(6) Fuel-fuel and fuel-cladding interaction → fuel-fuel interaction only

For this case we have

$$\delta^{\xi}_{f2} = (1/D_2) \sum_c M^{\xi}_k \tag{3.54}$$

where D_2 was defined in case (5).

Next,

$$\left.\begin{aligned} \delta^{\xi}_{f1} &= \left[\frac{D_b}{D_b + D_{f1}}\right] \delta^{\xi}_{f2} \\ \delta^{\xi}_{b} &= \delta^{\xi}_{f2} - \delta^{\xi}_{f1} \\ \delta^{\xi}_{c} &= -(D_2/D_c)\, \delta^{\xi}_{f2} \end{aligned}\right\} \tag{3.55}$$

(7) Fuel-cladding interaction → fuel-fuel and fuel-cladding interaction

For this case, we have

$$\left.\begin{aligned} \delta^{\xi}_{f2} &= -\gamma_b \left[\frac{D_{f1}}{D_{f1} + D_6}\right] (\kappa^{\xi}_{f2_o} - \kappa^{\xi}_{f1_o}) \\ \delta^{\xi}_{f1} &= \gamma_b \left[\frac{D_6}{D_{f1} + D_6}\right] (\kappa^{\xi}_{f2_o} - \kappa^{\xi}_{f1_o}) \\ \delta^{\xi}_{c} &= \left[\frac{D_a}{D_c + D_a}\right] \delta^{\xi}_{f2} \\ \delta^{\xi}_{a} &= \delta^{\xi}_{c} - \delta^{\xi}_{f2} \\ \kappa^{\xi}_{bo} &= \left\{1 - \gamma_b \left[\frac{\eta_b D_{f1} + D_6}{\eta_b (D_{f1} + D_6)}\right]\right\} (\kappa^{\xi}_{f2_o} - \kappa^{\xi}_{f1_o}) \end{aligned}\right\} \tag{3.56}$$

where D_6 is given by

$$D_6 = [D_{f2} + \frac{D_a D_c}{D_a + D_c}] \quad .$$

(8) Fuel-fuel and fuel-cladding interaction → fuel-cladding interaction only

In this case,

$$\left.\begin{aligned} \delta^{\xi}_{f1} &= - (1/D_{f1}) \sum_{f1} M^{\xi}_{k} \\ \delta^{\xi}_{f2} &= - (D_{f1}/D_6) \delta^{\zeta}_{f1} \end{aligned}\right\} \qquad (3.57)$$

$$\delta^{\xi}_{c} = [\frac{D_a}{D_c + D_a}] \delta^{\zeta}_{f2}$$

$$\delta^{\xi}_{a} = [\frac{- D_c}{D_c + D_a}] \delta^{\xi}_{f2}$$

where D_6 was defined in the above case.

(9) No interaction → fuel-fuel and fuel-cladding interaction

This case and the remaining cases can be obtained by combining previous cases. In each of the remaining cases, the fuel-fuel interaction and fuel-cladding interaction both change during the time step and the order in which these two changes are assumed to occur may influence the final result. In the case considered here (i.e. both fuel-cladding and fuel-fuel interaction established) it will be assumed that the fuel-fuel interaction is established first. First apply case (3) to obtain the updated values for the initial curvatures of fuel zones 1 and 2 and the initial curvature of the fuel-fuel interaction element. Next, apply case (5) to again update the fuel zone curvatures, update the cladding and fuel-fuel interaction element curvatures, and set the initial value of the fuel-cladding interaction element.

(10) Fuel-fuel and fuel-cladding interaction → no interaction

In this case it will be assumed that the fuel-cladding interaction is broken first and then the fuel-fuel interaction is broken. First apply case (6) and then apply case (4).

(11) Fuel-fuel interaction only → fuel-cladding interaction only

It will somewhat arbitrarily be assumed that fuel-cladding interaction is established and then fuel-fuel interaction is broken. First apply case (5) and then apply case (8).

(12) Fuel-cladding interaction only → fuel-fuel interaction only

Finally, assume fuel-cladding interaction is broken first and then fuel-fuel interaction is established. Apply case (2) and then apply case (3).

D. Post-Time-Step Processing

After the increments in the cladding curvatures and axial strain have been calculated from the finite element solution procedure it is necessary to back-calculate the curvature and axial strain increments in the fuel and the curvature increments in the interaction elements. In addition, the stress increments in the fuel and cladding rings and in the interaction elements must also be calculated.

The fuel zone and interaction element strain increments are given by Equations (3.30), (3.31), (3.33), (3.34), (3.36), (3.38), (3.39) and (3.41). Once the fuel and cladding strain increments have been calculated, the stresses in the individual rings can be calculated. The moment and axial force increments in the rings are given by Equations (3.12), (3.13), and (3.14). The moment increments in the interaction elements are given by Equations (3.23), (3.24), (3.26) and (3.27) if there is interaction, otherwise, these moments are set to zero. If the fuel is single-zone, the curvatures and axial strain in fuel zone 1 and the curvatures of the fuel-fuel interaction element are not calculated.

E. Summary

In summary, a fuel rod incremental constitutive equation of the form

$$\begin{bmatrix} \Delta M^x \\ \Delta M^y \\ \Delta T \end{bmatrix} = \begin{bmatrix} D_{11} & 0 & 0 \\ 0 & D_{22} & 0 \\ 0 & 0 & D_{33} \end{bmatrix} \begin{bmatrix} \Delta \kappa^x \\ \Delta \kappa^y \\ \Delta \varepsilon \end{bmatrix} + \begin{bmatrix} E_1 \\ E_2 \\ E_3 \end{bmatrix}$$

has been derived. The particular values of the D's and E's used depends upon the state of contact interaction between the fuel zones and the cladding.

(1) No fuel-fuel or fuel-cladding contact → Use (3.29).

(2) Fuel-cladding interaction only → Use (3.32).

(3) Fuel-fuel interaction only → Use (3.35).

(4) Fuel-fuel and fuel-cladding contact → Use (3.40).

If the interaction state changes during a time step, modify the constitutive equation using (3.43). The value of δ to use in (3.43) depends upon how the interaction state changed. Values for δ for the twelve ways that the state can change were given by Equations (3.49) - (3.57).

IV. The Induced Curvatures

In the formulation of the ring constitutive equations in Section III it was mathematically convenient to use the concept of "induced" curvatures. An induced curvature is defined to be a curvature which would occur in a ring if there were no bending moments acting within the ring. In other words, it is the moment-free curvature (or curvature rate) at an axial location of a CYGRO ring. A number of different mechanisms have been identified which can cause a moment-free curvature of a fuel rod and these are discussed in this section. All of the curvature contributions discussed here are included in one-dimensional form in the current version of the ROBOT program [2]. This section serves to document the current methods for calculating these induced curvature contributions and to extend the methods so that curvatures in the x-z and y-z planes can be calculated simultaneously. All of the material behavior models used in the calculation of these curvatures are identical to the corresponding models used in the CYGRO program. Constants appearing in these models have values which are the same as determined for use in CYGRO.

Figure 6 shows two cross-sections of a CYGRO ring element. As shown, points P_{x1}, P_{x2}, P_{y1} and P_{y2} are located on the average ring radius and on the x and y coordinate lines. Differences in the axial strains at these points will cause the ring to bend in the x-z and y-z planes. If it is assumed that plane cross-sections remain plane during bending, the curvature increments induced in the ring are given by

$$\Delta\kappa^{xi} = (\Delta\varepsilon_z^{P_{x1}} - \Delta\varepsilon_z^{P_{x2}})/d \tag{4.1}$$

$$\Delta\kappa^{yi} = (\Delta\varepsilon_z^{P_{y1}} - \Delta\varepsilon_z^{P_{y2}})/d \tag{4.2}$$

where $\Delta\varepsilon_z^{P_{x1}}$, $\Delta\varepsilon_z^{P_{x2}}$, $\Delta\varepsilon_z^{P_{y1}}$ and $\Delta\varepsilon_z^{P_{y2}}$ are the axial strain increments at points P_{x1}, P_{x2}, P_{y1} and P_{y2} respectively, d is the average ring diameter (= outer radius + inner radius), and where second-order strain terms have been neglected. The strain increments in Equations (4.1) and (4.2) are each a sum of strain increment contributions from various mechanisms such as stress-free growth and thermal expansion. From Equations (4.1) and (4.2), the total induced curvature increments can be written as

$$\Delta\kappa^{xi} = \sum_\alpha \Delta\kappa_\alpha^{xi} \tag{4.3}$$

$$\Delta\kappa^{yi} = \sum_\alpha \Delta\kappa_\alpha^{yi} \tag{4.4}$$

where $\Delta\kappa_\alpha^{xi}$ and $\Delta\kappa_\alpha^{yi}$ are the curvature increments from the αth mechanism and are given by

$$\Delta\kappa_\alpha^{xi} = (\Delta\varepsilon_{z\alpha}^{P_{x1}} - \Delta\varepsilon_{z\alpha}^{P_{x2}})/d \tag{4.5}$$

$$\Delta\kappa_\alpha^{yi} = (\Delta\varepsilon_{z\alpha}^{P_{y1}} - \Delta\varepsilon_{z\alpha}^{P_{y2}})/d \tag{4.6}$$

where $\Delta\varepsilon_{z\alpha}^{P_{x1}}$, $\Delta\varepsilon_{z\alpha}^{P_{x2}}$, $\Delta\varepsilon_{z\alpha}^{P_{y1}}$, and $\Delta\varepsilon_{z\alpha}^{P_{y2}}$ are the strain increments associated with the αth mechanism. The various types of induced curvatures will now be discussed.

A. Fuel Swelling Curvature (Fuel Rings)

The z-direction strain due to fuel swelling is given by

$$\varepsilon_z = R_z C_1 S(P, T) [C_2 f + (1-p)^2 C_3 V_s (f,(1-p))] \quad (4.7)$$

where

R_z = z-direction strain director

C_1, C_2, C_3 = constants

P = hydrostatic pressure

T = temperature

S = tabular function of P and T

f = depletion

p = porosity

V_s = tabular function of (f/(1-p)).

If there is a fission rate gradient across the fuel rod, the depletions at the points P_{x1}, P_{x2}, P_{y1} and P_{y2} will be different and therefore the z-direction strains due to swelling will be different at these points. The depletions at the four points can be calculated from the nominal fission rate and the fission rate gradient. These depletions are then used in Equation (4.7) to calculate the z-direction strains. Performing this calculation for the beginning and end of the time step and taking the difference in the calculated strains gives the strain increment for each of the four points. These strain increments are then used in (4.3) and (4.4) to obtain the curvature increment.

B. Fuel Densification Curvature (Fuel Rings)

The fuel densification z-direction strain rate is given by

$$\dot{\varepsilon}_z = R_z \sum_h \dot{\varepsilon}_h$$

where R_z is the z-direction strain director and $\dot{\varepsilon}_h$ is the volumetric strain rate associated with the hth pore class and is given by

$$\dot{\epsilon}_h = \frac{-1}{\eta} \{\gamma [4.5 \pi N_s (1-\epsilon_h) \epsilon_h^2]^{1/3} + P(\epsilon_h) + S_y \epsilon_h \ln \epsilon_h\} \quad (4.8)$$

where

ϵ_h = volume fraction of pore class h

η = effective viscosity obtained from the steady-state creep equations

N_s = number density of the pores in class h

γ = surface tension

S_y = constants .

The function $P(\epsilon_h)$ is given by

$$P(\epsilon_h) = -\frac{3}{8} [(\sigma_r + \sigma_\theta + \sigma_z)/\ln (1+V_{sol}/\epsilon_h)]$$

where

σ_r, σ_θ, σ_z = stresses

V_{sol} = solid volume fraction associated with the pore.

The effective shear viscosity η depends upon the fission rate. If there is a transverse gradient of the fission rate, η and ϵ_h will be different at the points P_{x1}, P_{x2}, P_{y1} and P_{y2}. Thus, the densification strain rates at these points will be different, thereby inducing a curvature rate in the ring.

The procedure for calculating the curvature increment is as follows. The fission rates at P_{x1}, P_{x2}, P_{y1} and P_{y2} are calculated from the nominal fission rate and the fission rate gradient. The effective shear viscosity η is calculated for each of the four points and then Equation (4.8) is integrated over the time step to obtain the updated value of ϵ_h and $\Delta\epsilon_h$. Summing the $\Delta\epsilon_h$'s at points P_{x1}, P_{x2}, P_{y1} and P_{y2} gives the total densification strain increment at each of these points. The strain increments are then used to obtain the curvature increments using (4.5) and (4.6).

C. Fission Rate Gradient Curvature (Fuel Rings)

In the fuel the creep strain rate's dependence upon the fission rate is given by

$$\dot{\varepsilon}_z = G_z [\dot{\varepsilon}_o + Q \dot{f} \sigma_g] \tag{4.9}$$

where G_z is the z-direction strain director, $\dot{\varepsilon}_o$ is the generalized strain rate which would occur if the fission rate were zero, Q is a constant, $\dot{f}$ is the fission rate, and σ_g is the generalized stress. The transverse fission rate gradient causes the creep strain rates at points P_{x1}, P_{x2}, P_{x3} and P_{x4} to be different and thereby induces a curvature rate in the ring.

From (4.9), the axial strain rate at P_{x1} will be

$$\dot{\varepsilon}_1 = G_z [\dot{\varepsilon}_o + Q \sigma_g (\dot{f}_o - g_x r_{av})] \tag{4.10}$$

where $\dot{f}_o$ is the nominal centerline fission rate, g_x is the x-component of the fission rate gradient, and r_{av} is the average radius of the ring. Similarly, the axial strain rate at P_{x2} is given by

$$\dot{\varepsilon}_2 = G_z [\dot{\varepsilon}_o + Q \sigma_g (f_o + g_x r_{av})] . \tag{4.11}$$

Substituting (4.10) and (4.11) into the curvature equation (4.5) and multiplying by the time increment Δt gives

$$\Delta\kappa^{xi} = - G_z Q \sigma_g g_x \Delta t . \tag{4.12}$$

Similarly,

$$\Delta\kappa^{yi} = - G_z Q \sigma_g g_y \Delta t . \tag{4.13}$$

As a first-order approximation the generalized stress used in (4.12) and (4.13) will be the axisymmetric generalized stress calculated by CYGRO.

D. Cladding Eccentricity-Induced Curvatures (Cladding Rings)

If the cladding eccentricity is non-zero, it can be shown that the eccentricity-induced stress perturbations at points P_{x1}, P_{x2}, P_{y1} and P_{y2} are approximately given by:

Point P_{x1}

$$\delta\sigma_r = 0, \quad \delta\sigma_\theta = -\left(\frac{e_x}{t}\right)\sigma_\theta\Big|_{nom}, \quad \delta\sigma_z = -\left(\frac{e_x}{t}\right)\sigma_z\Big|_{nom} \tag{4.14}$$

Point P_{x2}

$$\delta\sigma_r = 0, \quad \delta\sigma_\theta = \left(\frac{e_x}{t}\right)\sigma_\theta\Big|_{nom}, \quad \delta\sigma_z = \left(\frac{e_y}{t}\right)\sigma_z\Big|_{nom} \tag{4.15}$$

Point P_{y1}

$$\delta\sigma_r = 0, \quad \delta\sigma_\theta = -\left(\frac{e_y}{t}\right)\sigma_\theta\Big|_{nom}, \quad \delta\sigma_z = -\left(\frac{e_y}{t}\right)\sigma_z\Big|_{nom} \tag{4.16}$$

Point P_{y2}

$$\delta\sigma_r = 0, \quad \delta\sigma_\theta = \left(\frac{e_y}{t}\right)\sigma_\theta\Big|_{nom}, \quad \delta\sigma_z = \left(\frac{e_y}{t}\right)\sigma_z\Big|_{nom} \tag{4.17}$$

where $\delta\sigma_r$, $\delta\sigma_\theta$ and $\delta\sigma_z$ are the stress perturbations, e_x and e_y are the x and y components of the eccentricity, $\sigma_\theta|_{nom}$ and $\sigma_z|_{nom}$ are the CYGRO-calculated axisymmetric circumferential and axial stresses, and t is the nominal cladding wall thickness in the absence of eccentricity. The stress perturbations given above cause perturbations in both the axial elastic strain and the axial creep strain rate.

The elastic strain increments due to the perturbational stress at P_{x1}, P_{x2}, P_{y1} and P_{y2} will be

$$\Delta\varepsilon_z^{P_{x1}} = \Delta\varepsilon\Big|_{nom} \left(-\frac{e_x}{t}\right) \tag{4.18}$$

$$\Delta\varepsilon_z^{P_{x2}} = \Delta\varepsilon\Big|_{nom} \left(\frac{e_x}{t}\right) \tag{4.19}$$

$$\Delta\varepsilon_z^{P_{y1}} = \Delta\varepsilon\Big|_{nom} \left(-\frac{e_x}{t}\right) \tag{4.20}$$

$$\Delta\varepsilon_z^{P_{y2}} = \Delta\varepsilon\Big|_{nom} \left(\frac{e_x}{t}\right) \tag{4.21}$$

where

$$\Delta\varepsilon\Big|_{nom} = \left(\Delta\sigma_z\Big|_{nom} - \upsilon\, \Delta\sigma_\theta\Big|_{nom}\right)/E \tag{4.22}$$

where υ is Poisson's ratio, E is Young's modulus, and $\Delta\sigma_z\Big|_{nom}$ and $\Delta\sigma_\theta\Big|_{nom}$ are the changes in the CYGRO-calculated axisymmetric stresses. Substituting (4.18) - (4.21) into (4.5) and (4.6) gives

$$\Delta\kappa^{xi} = -2\, \Delta\varepsilon\Big|_{nom} \left(\frac{e_x}{td}\right) \tag{4.23}$$

$$\Delta\kappa^{yi} = -2\, \Delta\varepsilon\Big|_{nom} \left(\frac{e_y}{td}\right) \tag{4.24}$$

for the elastic component of the eccentricity curvature. In the above equations, d is the average ring diameter.

If $\delta\sigma_i$ is the stress perturbation, the z-direction creep strain rate will be

$$\dot{\varepsilon}_z\,(\sigma_i + \delta\,\sigma_i) = \dot{\varepsilon}_z\,(\sigma_i) + \sum_{k=r,\theta,z} \left(\frac{\partial\,\dot{\varepsilon}_z}{\partial\,\sigma_k}\right) \delta\,\sigma_k\,.$$

During a time step Δt the creep strain increment due to the perturbational stress will be

$$\Delta\varepsilon_z = \sum_{k=r,\theta,z} \left(\frac{\delta\sigma_k}{V_k}\right) \Delta t$$

where

$$\frac{1}{V_k} = \left(\frac{\partial \dot{\varepsilon}_z}{\partial \sigma_k}\right) .$$

Using the stress perturbations given by (4.14) - (4.17), the perturbational creep strain increments at points P_{x1}, P_{x2}, P_{y1} and P_{y2} will be given by (4.18) - (4.21) but with $\Delta\varepsilon\big|_{nom}$ now given by

$$\Delta\varepsilon\Big|_{nom} = \left(\frac{\Delta t}{V_k}\right)\sigma_z\Big|_{nom} + \left(\frac{\Delta t}{V_\theta}\right)\sigma_\theta\Big|_{nom} \tag{4.25}$$

Substituting these strain increments into (4.5) and (4.6) gives

$$\Delta\kappa^{xi} = -2\,\Delta\varepsilon\Big|_{nom}\left(\frac{e_x}{td}\right) \tag{4.26}$$

$$\Delta\kappa^{yi} = -2\,\Delta\varepsilon\Big|_{nom}\left(\frac{e_x}{td}\right) \tag{4.27}$$

In summary, the cladding eccentricity induces an elastic and creep curvature increment in the ring. The elastic curvature increment is given by (4.23) and (4.24) with $\Delta\varepsilon\big|_{nom}$ given by (4.22). The creep curvature increment is given by (4.26) and (4.27) with $\Delta\varepsilon\big|_{nom}$ given by (4.25).

E. Thermal Expansion Curvature (Fuel and Cladding Rings)

In CYGRO the temperature distribution in the rod is assumed to be axisymmetric and the material properties and thermal expansion strains in each CYGRO ring are calculated using the average temperature for the ring. Transverse gradients in the non-axisymmetric component of the fission rate, the coolant temperature, or the cladding-coolant interface conductivity can cause the

temperature distribution to be non-axisymmetric, thereby inducing temperature-related curvatures in the rod. To calculate the temperature distribution, it is assumed that the non-axisymmetric component of the temperature is a perturbation of the symmetric temperature distribution calculated in CYGRO. Ring thermal conductivities associated with the axisymmetric temperature distribution are used to calculate the perturbational temperature distribution. The details of the calculation of the perturbational temperature distribution are given in Reference [1] for the case in which only x-direction gradients of the fission rate, coolant temperature, and clad-coolant thermal conductivity are present. Because of the linearity of the governing equations, the perturbational temperature distribution for the case in which the above gradients have both x and y components can be obtained by superposition. The procedure given in Reference [1] is applied twice, first using the x components of the gradients and then applied using the y components of the gradients. The two calculated temperature distributions are then superimposed to obtain the total perturbational temperature distribution.

Once the perturbational temperatures at points P_{x1}, P_{x2}, P_{y1} and P_{y2} are calculated, the z-direction thermal expansion strain is given by

$$\varepsilon_z = \int_{T_{ref}}^{T} k_z \, d\tau \tag{4.28}$$

where k_z is the z-direction coefficient of thermal expansion and T is the sum of the axisymmetric temperature and the perturbational temperature. The change in the thermal expansion strain will be

$$\Delta\varepsilon_z = \int_{T}^{T+\Delta T} k_z \, d\tau \tag{4.29}$$

where ΔT is the total temperature change during the time step. Evaluating (4.29) for points P_{x1}, P_{x2}, P_{y1} and P_{y2} and substituting into (4.5) and (4.6) gives the thermal expansion curvature increments.

F. Flux-Induced Stress-Free Growth Curvature (Cladding Rings)

In the constitutive equation for Zircaloy, the stress-free growth is a contribution to the total strain rate which depends on temperature and fast-neutron flux but is independent of the stress. Thus, this term represents a strain rate which can occur when the material is unstressed. Because the stress-free growth rate depends upon the temperature and the fast-neutron flux, transverse gradients of these quantities will cause the stress-free strain rates at points P_{x1}, P_{x2} P_{y1} and P_{y2} to be different. Thus, curvature components associated with stress-free growth can be induced in the cladding rings.

The z-direction strain rate associated with the stress-free growth is given by

$$\dot{\varepsilon}_z = \dot{\varepsilon}_v + R_z \dot{\varepsilon}_\ell \tag{4.30}$$

where $\dot{\varepsilon}_v$ is an isotropic strain rate component, R_z is the z-direction strain director, and $\dot{\varepsilon}_\ell$ is the shape change component of the growth. The isotropic strain rate component is given by

$$\dot{\varepsilon}_v = \{S_v \left[\frac{\phi}{\phi + \phi_o} \exp\left(\frac{Q_v}{T}\right)\right]^{1/2} - \varepsilon_v\} \left[C_v \phi + D_v \exp\left(\frac{-Q_v}{T}\right)\right] \tag{4.31}$$

where S_v, ϕ_o, Q_v, C_v and D_v are constants, ϕ is fast-neutron flux, and T is absolute temperature. The shape change component is the sum of a transient term and a steady-state term, i.e.

$$\dot{\varepsilon}_\ell = \dot{\varepsilon}_t + \dot{\varepsilon}_s \tag{4.32}$$

where

$$\dot{\varepsilon}_t = \left[S_\ell \{1 - \exp\left(-Q_\ell \left[\frac{1}{T} - \tau_\ell\right]\right)\} \frac{C_t \phi}{\phi + \phi_o} - \varepsilon_t\right] \frac{\phi}{F_z} \tag{4.33}$$

$$\dot{\varepsilon}_s = S_\ell \{1 - \exp(-Q_\ell [\tfrac{1}{T} - \tau_\ell])\} (C_z + H) \phi \tag{4.34}$$

$$H = \begin{cases} 0 \quad \text{for} \quad \int_0^t \phi \, dt \leq \Psi^* \\ (\frac{A_z}{B_z} - H) \frac{\phi}{B_z} \quad \text{otherwise} . \end{cases} \tag{4.35}$$

where S_ℓ, Q_ℓ, τ_ℓ, C_t, F_z, A_z, B_z, and Ψ^* are constants.

The strain increments at points P_{x1}, P_{x2}, P_{y1}, and P_{y2} are calculated by numerically integrating Equations (4.30) - (4.35) from t_1 to $t_1 + \Delta t$ at each point using the fast-neutron flux and temperature appropriate for each point. The temperature which is used is the sum of the axisymmetric temperature and the perturbational temperature. To integrate the above equations it is necessary to keep track of the values of H and ε_v at P_{x1}, P_{x2}, P_{y1} and P_{y2}. The strain increments which are calculated are then used in (4.5) and (4.6) to calculate the stress-free growth curvature increments.

G. Fast-Neutron Flux Gradient Curvature (Cladding Rings)

The creep rate of Zircaloy depends upon the fast-neutron flux. If there is a transverse gradient of the fast-neutron flux, one side of a cladding ring will creep faster than the other and a curvature contribution will be induced in the ring.

At point P_{x1} the creep rate will be

$$\dot{\varepsilon}_z^{P_{x1}} = [\dot{\varepsilon}\Big|_{nom} - (\frac{\partial \dot{\varepsilon}}{\partial \phi})(\frac{\partial \phi}{\partial x}) r_{av}] G_z \tag{4.36}$$

where $\dot{\varepsilon}\Big|_{nom}$ is the creep rate which would exist if there were no fast-neutron flux gradient, ϕ is fast-neutron flux, r_{av} is the average ring radius, and G_z is the z-direction strain director. Similarly, the creep rate at P_{x2} will be

$$\dot{\varepsilon}_z^{P_{x2}} = \left[\dot{\varepsilon}\Big|_{nom} + \left(\frac{\partial \dot{\varepsilon}}{\partial \phi}\right)\left(\frac{\partial \phi}{\partial x}\right) r_{av}\right] G_z \quad . \tag{4.37}$$

The strain increments at P_{x1} and P_{x2} are obtained by multiplying (4.36) and (4.37) by the time increment Δt. From (4.5), the curvature increment will be

$$\Delta\kappa^{xi} = -\left(\frac{\partial \dot{\varepsilon}}{\partial \phi}\right)\left(\frac{\partial \phi}{\partial x}\right) G_z \, \Delta t \quad . \tag{4.38}$$

Similarly, for the y direction,

$$\Delta\kappa^{yi} = -\left(\frac{\partial \dot{\varepsilon}}{\partial \phi}\right)\left(\frac{\partial \phi}{\partial y}\right) G_z \, \Delta t \quad . \tag{4.39}$$

V. Calculation of the Initial Free Shape of the Fuel Rod Neutral Axis

Initially, the neutral axis of bending of the fuel rod will be the centroidal axis of the cladding. The location of the centroidal axis is determined by the lateral deflection of the cladding center and by the x and y values of the cladding eccentricity. The values of the cladding center deflection and eccentricity are usually known at discrete points along the length of the fuel rod. The problem is to find a set of initial nodal displacements which yield an initial shape which best fits the initial centroidal shape data. In what follows, a method for obtaining a least-squares curve fit to the data using the finite element shape functions is developed. The procedure is somewhat complicated by the fact that the deflection and eccentricity data are not generally known at the same set of axial locations.

In the finite element description of the rod shape, the shape is determined by the values of the nodal deflections $\underline{P}$. In particular, within each element the lateral deflection is given by

$$\begin{bmatrix} u \\ v \end{bmatrix} = \begin{bmatrix} S_u^i \\ \hline S_v^i \end{bmatrix} \begin{bmatrix} P_1 \\ \vdots \\ P_{10} \end{bmatrix}$$

where S_u^i and S_v^i are the first two rows of the shape matrix of the ith element. There is no need to include the axial deflections. Next, suppose that there is a set of data points X_{ij} and Y_{ij} which represent the x- and y-deflection, respectively, of the jth data point within the ith element. Then, for the ith element, the sum of the squares of the differences between the data and the assumed shape will be

$$\mathcal{J}_i = \sum_j \{[X_{ij} - [S_u^{ij}]\ [P_i]]^2 + [Y_{ij} - [S_v^{ij}]\ [P_i]]^2\}$$

where $[S_u^{ij}]$ and $[S_v^{ij}]$ are the x- and y-direction shape functions of the ith element evaluated at the axial location corresponding to the jth data point. Summing over all elements (and therefore over all data points), we obtain

$$\mathcal{J} = \sum_i \sum_j \{[X_{ij} - [S_u^{ij}]\ [P_i]]^2 + [Y_{ij} - [S_v^{ij}]\ [P_i]]^2\}$$

We now want to miminize $\mathcal{J}$. To do this we set the partial derivative of $\mathcal{J}$ with respect to P_k to zero to obtain

$$-2 \sum_i \sum_j \{[X_{ij} - [S_u^{ij}]\ [P_i]]\ [S_u^{ij}]_{(k)} + [Y_{ij} - [S_v^{ij}]\ [P_i]]\ [S_v^{ij}]_{(k)}\} = 0 \qquad (5.1)$$

where $[\cdot]_{(k)}$ denotes the kth component of the matrix $[\cdot]$. Next, the matrix products $[S_u^{ij}]\,[P_i]$ and $[S_v^{ij}]\,[P_i]$ can be written in component form as $[S_u^{ij}]_{(\ell)}\,[P_i]_{(\ell)}$ and $[S_v^{ij}]_{(\ell)}\,[P_i]_{(\ell)}$, where a summation over the index ℓ is implied. Using this, equation (5.1) can be written in the form

$$\sum_i \sum_j \{[[S_u^{ij}]_{(k)}\,[S_u^{ij}]_{(\ell)} + [S_v^{ij}]_{(k)}\,[S_v^{ij}]_{(\ell)}]\,[P_i]_{(\ell)}\}$$

$$= \sum_i \sum_j \{[S_u^{ij}]_{(k)}\,X_{ij} + [S_v^{ij}]_{(k)}\,Y_{ij}\}$$

which can be written

$$\sum_i \{[\bar{K}_i]_{(k)(\ell)}\,[P_i]_{(\ell)}\} = \sum_i \{[\bar{F}]_{(k)}\} \tag{5.2}$$

where

$$[\bar{K}_i]_{(k)(\ell)} = \sum_j \{[S_u^{ij}]_{(k)}\,[S_u^{ij}]_{(\ell)} + [S_v^{ij}]_{(k)}\,[S_v^{ij}]_{(\ell)}\} \tag{5.3}$$

$$[\bar{F}]_{(k)} = \sum_j \{[S_u^{ij}]_{(k)}\,X_{ij} + [S_v^{ij}]_{(k)}\,Y_{ij}\} \tag{5.4}$$

Note that the equation

$$[\bar{K}_i]\,[P_i] = [\bar{F}]$$

looks very similar to an element stiffness equation. In fact, the summation over all of the elements indicated in Equation (5.2) is exactly the same as the finite element assembly procedure. This assembly procedure will produce a matrix equation of the form

$$\bar{\underset{\sim}{K}}\,\underline{P} = \underline{\bar{F}} \tag{5.5}$$

which is then solved to obtain $\underline{P}$. The matrix $\underset{\sim}{\overline{K}}$ will have the same properties as the global stiffness matrix; i.e. it will be banded, symmetric, and positive definite. This means that beyond the point where the element stiffness and force matrices are calculated, the finite element solution procedure can be re-used to calculate the initial nodal deflections. Therefore, to calculate the initial displacements, Equation (5.3) is used to calculate the element stiffness matrix and Equation (5.4) is used to calculate the element force vector. The subroutines which calculate these quantities would be called in place of the usual stiffness and force subroutines.

There is, however, a difficulty which can arise with the above procedure. The nodal displacements at a particular node only influence the shape of the curve in the elements joined to that node. This means that if there are no data points in those elements connected to the node, the nodal displacements are not uniquely determined and the $\overline{K}$ matrix will be singular. Thus, for the above procedure to work there must always be a sufficient number of data points in each element.

To get around this difficulty, it is assumed that the rod has a small amount of stiffness in bending and that instead of minimizing $\underset{\sim}{\delta}^0$, we will minimize the functional $\mathcal{H}$, given by

$$\mathcal{H} = \mathcal{S} + \mathcal{E}$$

where $\mathcal{E}$ is the elastic strain energy due to bending. The idea here is to make the bending stiffness very small so that $\mathcal{E}$ is very small compared to $\mathcal{S}$. If $\mathcal{S}$ dominates, then the set of nodal parameters which minimize $\mathcal{H}$ will be essentially the same as the set of parameters which minimize $\mathcal{S}$. In addition, when there are not enough data points in a region to uniquely define a minimum for $\mathcal{S}$, a unique minimum for $\mathcal{H}$ will exist because the nodal values will be such that they minimize the local strain energy. Thus, in regions where there is insufficient data, the curve will be uniquely defined and smooth.

To minimize $\mathcal{H}$, we have

$$\frac{\partial \mathcal{H}}{\partial P_i} = \frac{\partial \mathcal{S}}{\partial P_i} + \frac{\partial \mathcal{E}}{\partial P_i} = 0 . \tag{5.6}$$

From the least-squares analysis above we have

$$\frac{\partial \mathcal{S}}{\partial P_i} = \underset{\sim}{\overline{K}}\, \underline{P} - \underline{\overline{F}} \tag{5.7}$$

where $\underset{\sim}{\overline{K}}$ and $\underline{\overline{F}}$ are the same as in (5.5). Next, we assume that the beam has a fictitious elastic constitutive equation of the form

$$\underline{\Delta\sigma} = c\, \underset{\sim}{1}\, \underline{\Delta\varepsilon} \tag{5.8}$$

where $\underset{\sim}{1}$ is the identity matrix and c is a adjustable stiffness constant which can be used to make $\mathcal{E}$ small relative to $\mathcal{S}$. It can be shown that for a linearly elastic beam

$$\frac{\partial \mathcal{E}}{\partial P_i} = \underset{\sim}{\tilde{K}}\, \underline{P} \tag{5.9}$$

where $\underset{\sim}{\tilde{K}}$ is the global stiffness matrix obtained using the virtual work or Galerkin formulation of the finite element method. This means that the matrix $\underset{\sim}{\tilde{K}}$ in (5.9) can be obtained using the finite element formulation developed in Section II with (5.8) as the constitutive equation and with the initial nodal displacements set to zero to eliminate the nonlinearities. Substituting (5.7) and (5.9) into (5.6) gives

$$[\underset{\sim}{\overline{K}} + \underset{\sim}{\tilde{K}}]\, \underline{P} = \underline{\overline{F}} . \tag{5.10}$$

This equation can be set up by assembling finite elements whose stiffness equations are of the form

$$[\underset{\sim}{\overline{K}}_i + \underset{\sim}{\tilde{K}}_i]\, \underline{P}_i = \underline{\overline{F}}_i$$

where $\overline{\underset{\sim}{K}}_i$ and $\underline{F}_i$ are given by Equations (5.3) and (5.4) and where $\tilde{\underset{\sim}{K}}_i$ is the element stiffness matrix obtained when the beam has the elastic constitutive equation (5.8). Thus, the computer routines used for the structural calculations can still be used to calculate the initial free shape of the rod. It is only necessary to modify the routine that calculates the element stiffness equation.

The purpose of the above procedure is to calculate the initial shape of the rod's centroid. However, the centroidal deflection is not measured directly, but rather, it is the centerline deflection and the eccentricity which are known. If the centerline deflection and the eccentricity measurement were always taken at corresponding axial locations, the centroidal deflection at those locations could be calculated and the curve-fitting procedure described above could be used directly. Unfortunately, the locations at which the centerline deflection and eccentricity measurements are taken do not always correspond and additional interpolations are required. One method for calculating the initial centroidal free-shape for such data is to perform the least-squares curve fit twice. The first time through, a least-squares curve fit is obtained for the centerline deflection. This curve is now used to approximate the centerline deflection at points where the eccentricity is known. The centroidal deflection can then be calculated at these points using the formulae:

$$x = d_x - \frac{e_x(r_o - \tau)^2}{\tau(2r_o - \tau)}$$

$$y = d_y - \frac{e_y(r_o - \tau)^2}{\tau(2r_o - \tau)}$$

where x and y are the coordinates of the centroidal axis, d_x and d_y are the coordinates of the centerline, e_x and e_y are the x- and y-components of the eccentricity as shown in Figure 7, r_o is the clad outer radius, and τ is the nominal cladding thickness. Now, a least-squares curve fit can be obtained using this centroidal deflection data. The least-squares curve-fitting procedure described previously is simply repeated using the new data. The nodal displacements which are calculated will be the initial values of the nodal displacements and subsequent displacement increments will be added to these values.

VI. Summary

A numerical procedure for calculating the in-pile bowing of nuclear fuel rods has been formulated. The fuel rod is modeled as a viscoelastic beam whose deflections are solved for using an incremental finite element method. A computer program based on this procedure would work its way through the rod's history by taking small sequential time steps. For each time step, there are two main calculational parts. These are:

(1) the formulation of the rod's constitutive equations (i.e. the moment-curvature and axial force-strain relations), and

(2) the calculation of the rod's deflection increments using the finite element method.

The procedure for calculating the constitutive equations of the fuel rod is somewhat complex. First, for a given rod geometry and operational history, the CYGRO computer program is used to obtain a data file which contains histories of material properties and axisymmetric stresses and strains in the fuel rod. This data file is used to calculate some of the terms in the constitutive equations. Additional terms in these equations correspond to moment-free curvatures induced by transverse gradients of temperature and fast-neutron flux and by cladding circumferential wall thickness variations. These induced curvatures are calculated using material property models borrowed from the CYGRO program. The constitutive equations for each of the fuel zones and the cladding are then calculated using the CYGRO data file and the induced curvatures. An interaction model is used to combine these equations to form the constitutive equations which characterize the behavior of the fuel rod as a whole. The interaction model contains parameters called efficiencies which represent the degree of coupling between the fuel zones and between the fuel and the cladding. The values of some of these parameters can be approximately determined using out-of-pile deflection experiments.

Once the constitutive equations for the fuel rod have been determined for a time step, the incremental finite element equations can be formulated. The finite element formulation is nonlinear because of the coupling between the axial extension and the lateral deflection. The rod supports are modeled by specifying either force, displacement, flexible, or friction-type boundary conditions. The proposed finite element formulation results in a structure stiffness matrix which is symmetric and narrowly banded and can therefore be rapidly solved using a Cholesky-type equation solver.

References

1. J. B. Newman, "Inelastic Analysis of Bowing in Multispan Fuel Rods Subjected to Axial Thrust," Nuclear Engineering and Design, 9, 81-104 (1969).

2. J. J. Urbaniak, "ROBOT - A Computer Program to Solve the Bowing Problem in Rod-Type Fuel Elements," WAPD-TM-847, July 1969.

3. S. H. Crandall, "Engineering Analysis," McGraw-Hill, New York, 1956.

4. J. B. Newman, J. F. Giovengo, L. P. Comden, "The CYGRO-4 Fuel Rod Analysis Computer Program," WAPD-TM-1300, July 1977.

5. V. N. Faddeeva, "Computational Methods of Linear Algebra," Dover Publications, New York, 1959.

6. O. C. Zienkiewicz, "The Finite Element Method in Engineering Science," McGraw-Hill, London, 1971.

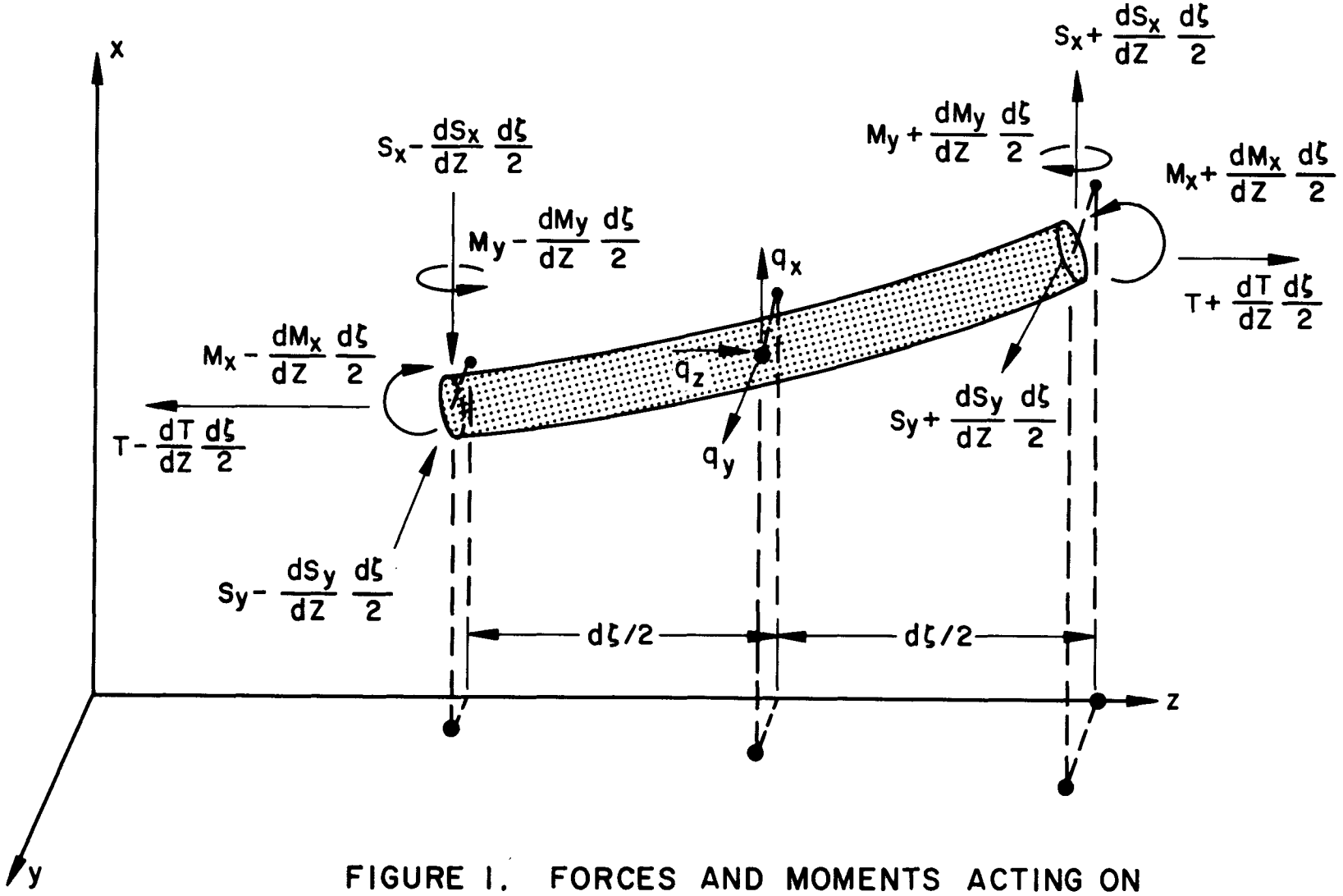

FIGURE 1. FORCES AND MOMENTS ACTING ON A DIFFERENTIAL BEAM ELEMENT

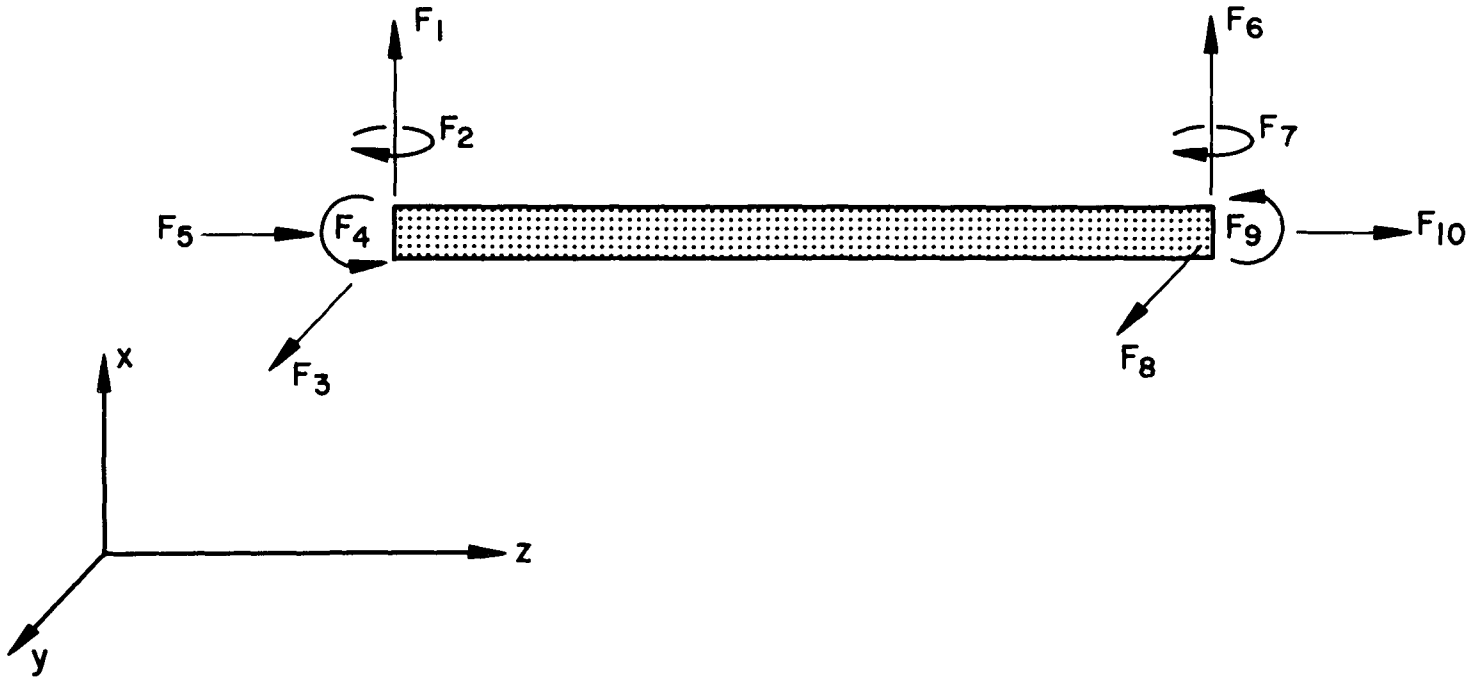

FIGURE 2. EXTERNAL FORCES AND MOMENTS APPLIED TO ENDS OF BEAM ELEMENT

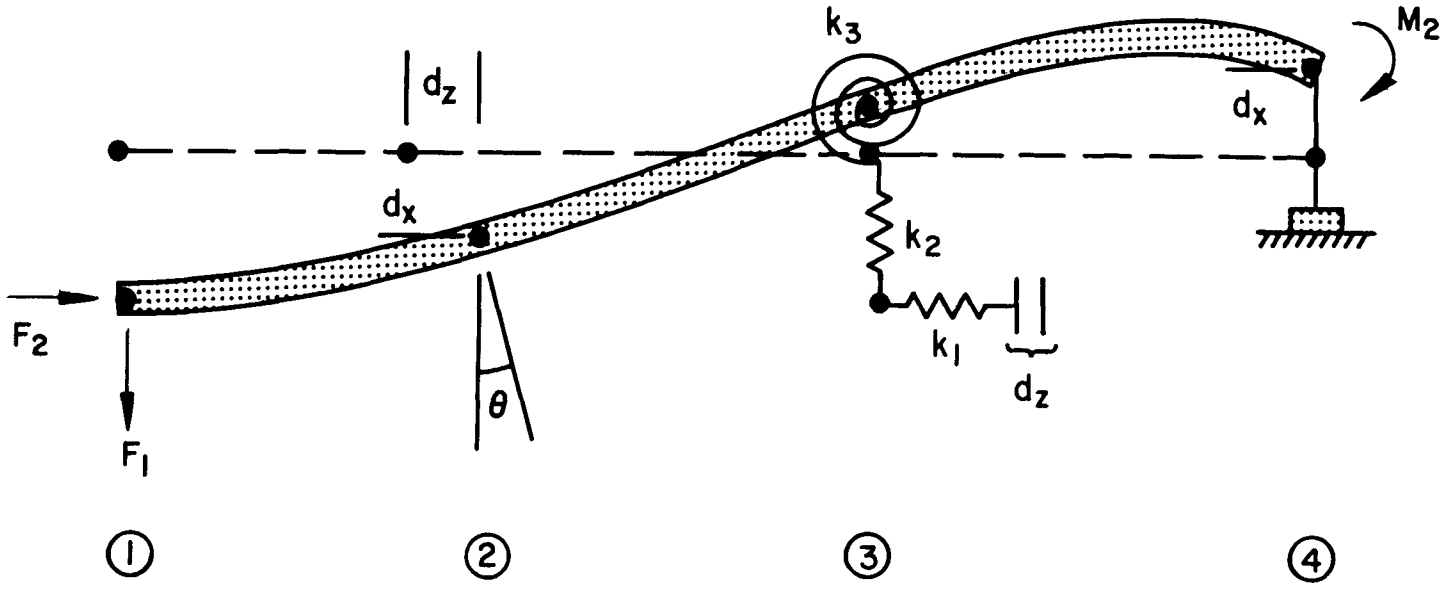

FIGURE 3. BOUNDARY CONDITION TYPES

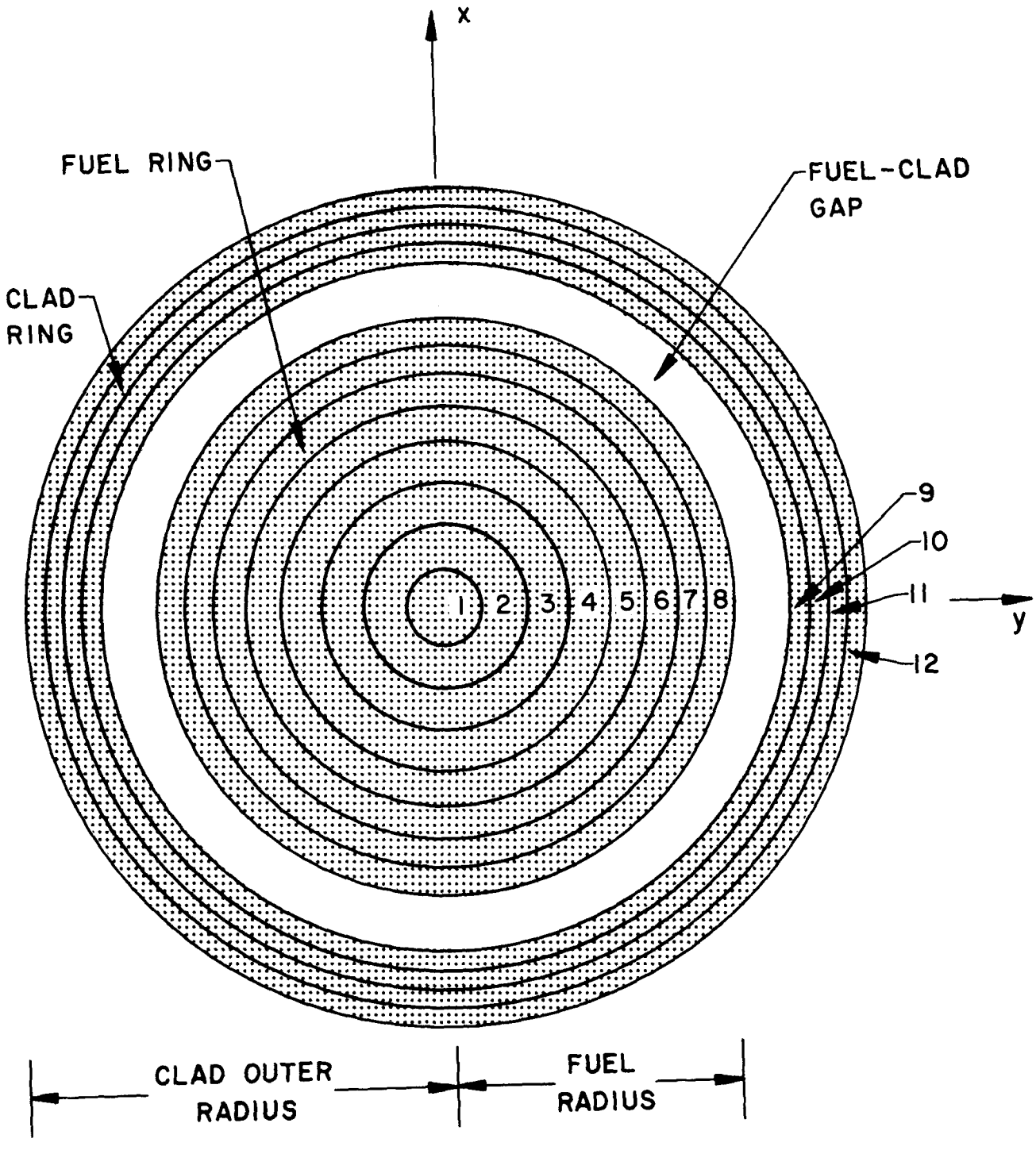

FIGURE 4. CYGRO'S RING TYPE FINITE ELEMENTS

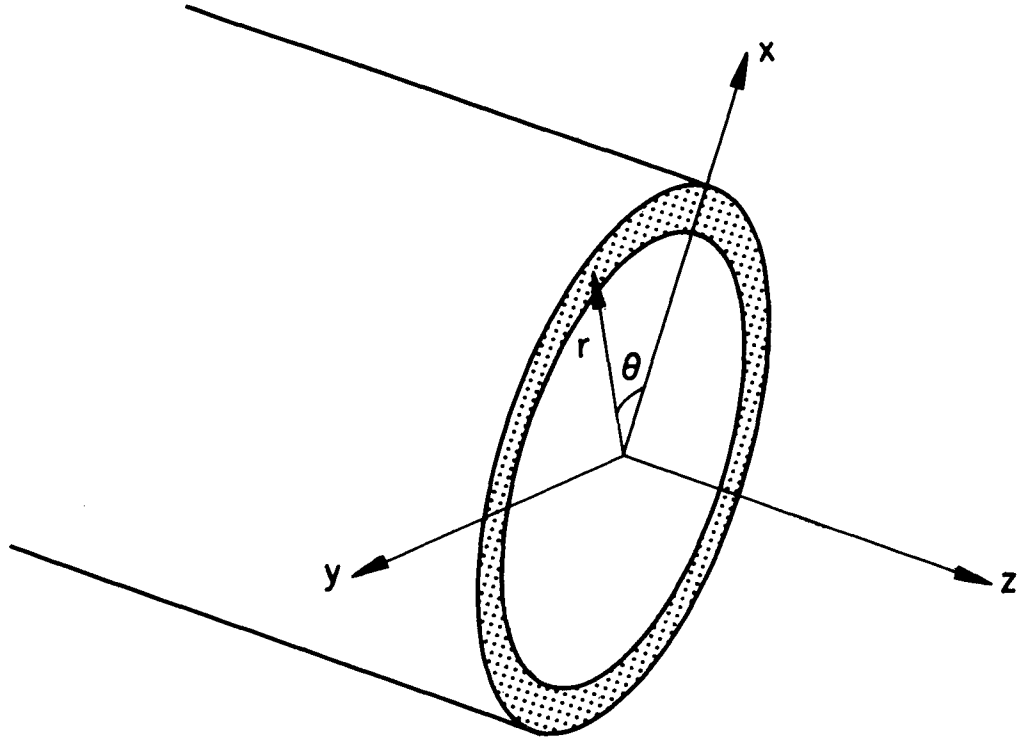

FIGURE 5. CARTESIAN AND CYLINDRICAL COORDINATES FOR A CYGRO RING

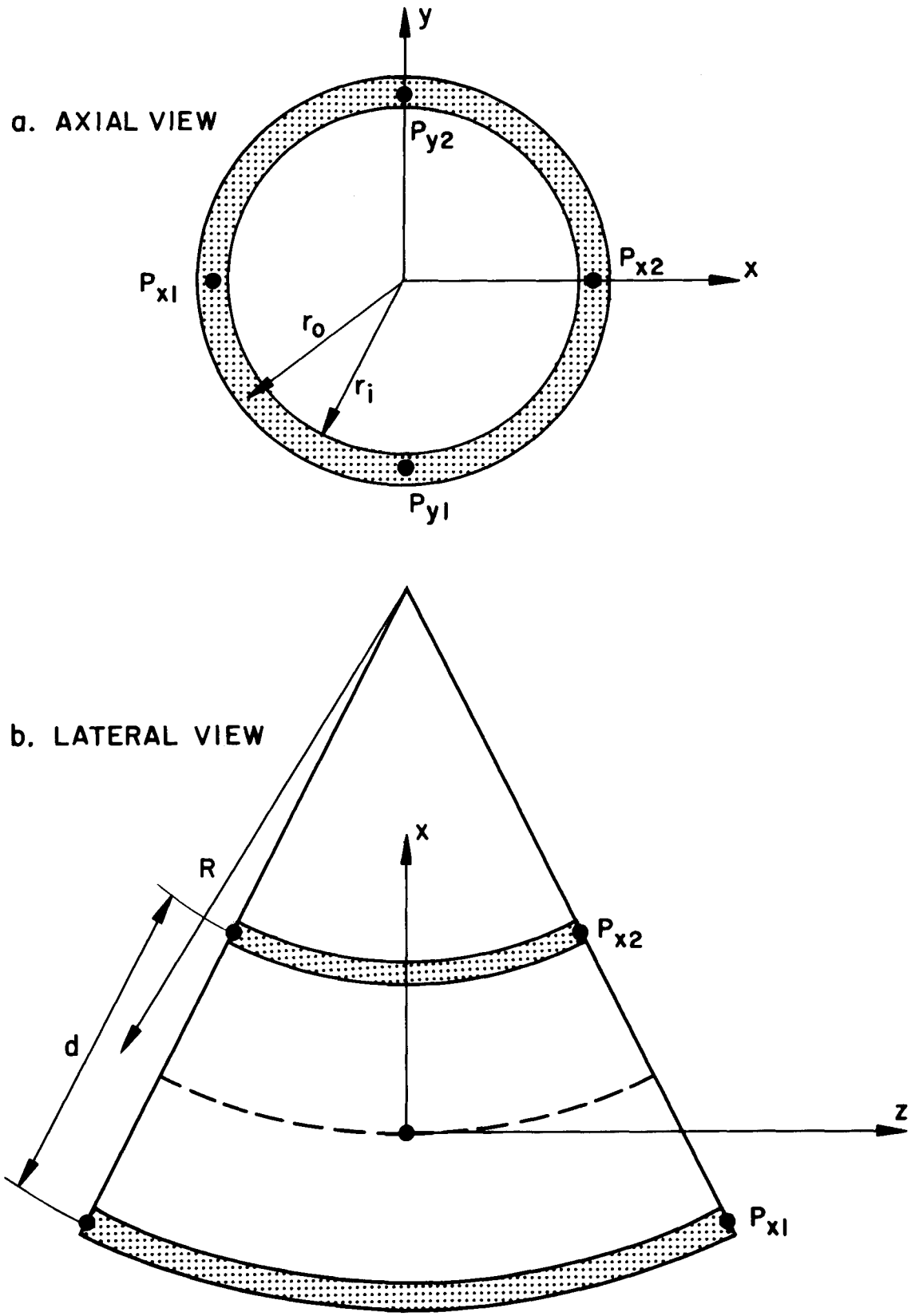

FIGURE 6. CYGRO RING CURVATURES

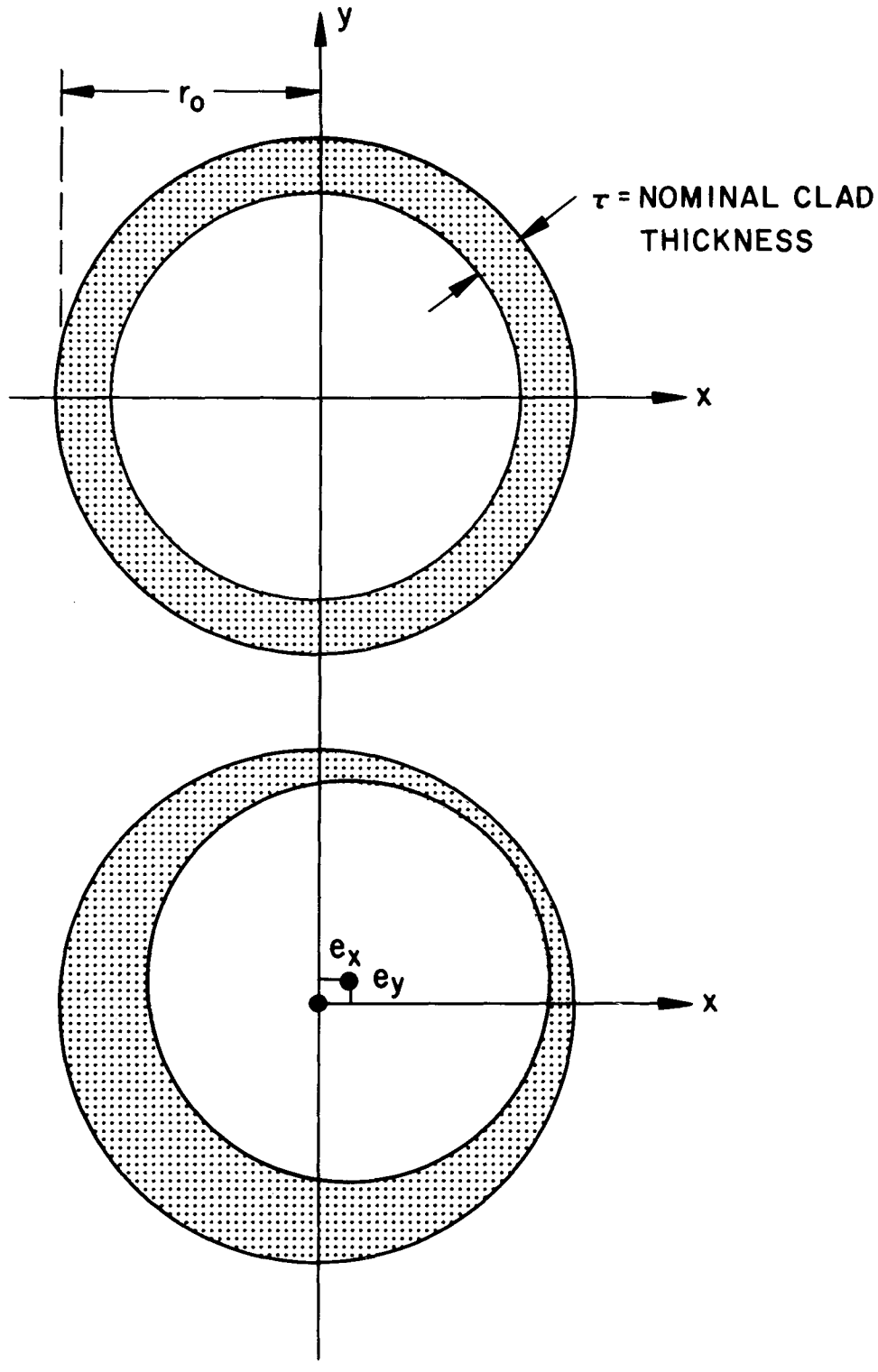

FIGURE 7. CLADDING ECCENTRICITY

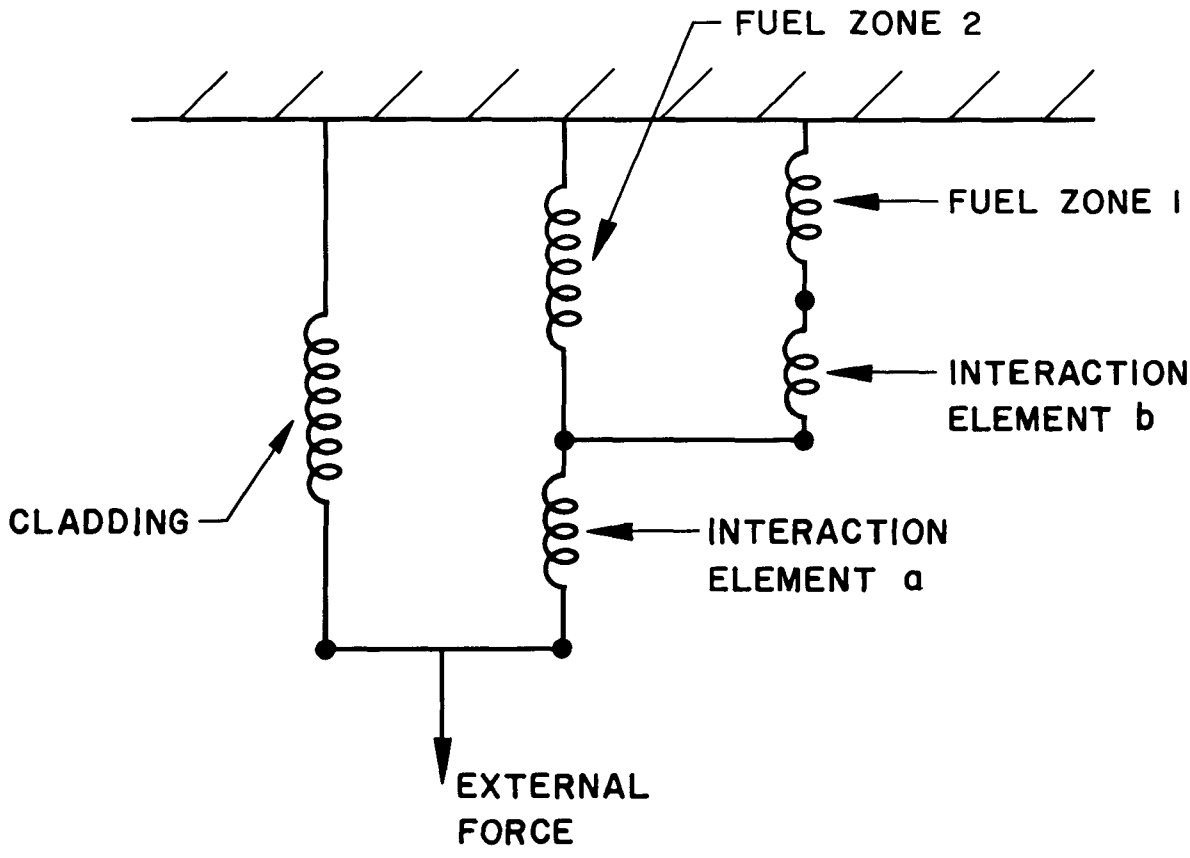

FIGURE 8. LINEAR SPRING ANALOG OF THE INTERACTION MODEL